THE ASTROPHYSICAL JOURNAL, 295:109–133, 1985 August 1

PROBING THE LUMINOUS STELLAR CORES OF THE GIANT H II REGIONS 30 DOR IN THE LMC AND NGC 3603 IN THE GALAXY

ANTHONY F. J. MOFFAT[1,2,3]
Département de physique, Université de Montréal
WILHELM SEGGEWISS[1]
Universitäts-Sternwarte Bonn, F. R. Germany
AND
MICHAEL M. SHARA[2]
Space Telescope Science Institute, Baltimore
Received 1984 July 2; accepted 1985 February 13

ABSTRACT

The stellar content of the two prototype (super) giant H II regions 30 Doradus and NGC 3603 is discussed on the basis of new (*a*) narrow- and wide-band CCD images of their central $3' \times 5'$ and (*b*) moderate resolution IDS spectroscopy of the central luminous object R136 = HD 38268 and other resolved Wolf-Rayet (W-R) stars in 30 Dor, and of the central luminous object HD 97950 in NGC 3603. We find:

1. A CCD in combination with narrow, 35 Å wide filters at 4650 Å (C IV) and 4686 Å (He II) versus a broad, 350 Å wide filter at 4700 Å is very effective in revealing *all* W-R stars (even strong-line Of stars) in a complex region. (The relatively rare W-R stars can be easily traced, as massive star probes, even in regions of high star density.) In addition, the filters serve well to separate WNL, WNE, and WCE stars. Beyond their bright central cores, only one potentially new W-R/Of candidate was uncovered in the central region of 30 Dor, while no new one was seen in NGC 3603 outside the dense core.

2. The overall radial surface brightness distribution in the wide filter satisfies the semiempirical King profile for spherically symmetric, isothermal stellar systems, over a span of two orders of magnitude in radius. The derived core radii are $r_c \approx 0.21$ pc (0″.82) for 30 Dor and $r_c \approx 0.024$ pc (0″.71) for NGC 3603. These radii are comparable to the seeing radius (HWHM) of 0″.65, indicating that the *true* core radii, if such do exist, could be much smaller than these derived values. In 30 Dor, the luminous WNL population is consistent with a King profile out to $r \approx 100$ pc. At the center of either region, nebular emission contributes very little to the total visual light. In 30 Dor, only about 20% of the total visual *or* ultraviolet light comes from a region within $r \approx 5''$ of R136a. The central objects of either region do not dominate the total stellar light output.

3. The central object R136a, and to a lesser degree HD 97950, show much broader wings in their radial surface brightness distributions than a single star. Subtraction of the background core light in either region yields $V \gtrsim 11.4$ ($M_v \gtrsim -8.4$) in R136 (extreme limits which are only slightly brighter than the nearby resolved WN6 stars R144 and R145 with $M_v = -8.0$ and -7.8 respectively, or even fainter if recent determinations of the distance of the LMC are correct) and $V \gtrsim 10.6$ ($M_v \gtrsim -8.0$) in HD 97950 for a central, unresolved object. Each of these is also multiple (e.g., astrometric components AB in R136 and AB in HD 97950), with no single star therefore likely brighter than $M_v \sim -7$ to -8. *Thus, there is no need to postulate a single star of extraordinarily high luminosity (or mass).*

4. The net emission image (4686 filter minus wide band filter, after nulling bright non–emission line stars) makes most of the (stellar, light-emitting) fuzz in and around R136 and HD 97950 disappear. There remains, however, an asymmetric stellar image, whose shape and intensity are best understood by the presence of more than one but not more than a few WN stars in each core ($\phi \lesssim 3''$).

5. Previously suspected spatial variations in the spectrum across the face of R136 and HD 97950 are confirmed by 2″ square aperture IDS spectroscopy. In the central $4'' \times 4''$, the mean visible spectrum is close to WN6 + O5 for both objects, with the He II emission lines stronger compared to N emission lines in the LMC object. The O type component resembles the mean spectrum of the surrounding resolved O stars in each case.

6. The only significant temporal variability of the spectra occurs in the periodic radial velocity (RV) of the W-R emission lines in each case. The RV amplitude is low compared to normal W-R binaries and likely results from dilution due to several W-R stars falling in the spectrograph aperture. The probability is high that at least one W-R star among a sample of 2 or more will exhibit RV duplicity. On this basis and with (4) and (5), we deduce that R136a contains ~4–5 WN stars, while HD 97950 contains ~2–3. The presence of massive tight binaries is important when considering the possibility of central core collapse in a dense cluster.

[1] Visiting astronomer, European Southern Observatory, Chile.
[2] Visiting astronomer, Cerro Tololo Inter-American Observatory, NOAO, Chile, operated by AURA, Inc., under contract with the NSF.
[3] Alexander von Humboldt Research Fellow, Universität Bonn 1982/83.

7. The ratio of the number of W-R stars to total light in R136 is similar to that in the surrounding cluster, NGC 2070. However, this ratio appears to be high in HD 97950 compared to NGC 3603, possibly as a result of more advanced relaxation in NGC 3603 (*if* small number statistics are unimportant). In 30 Dor and NGC 3603 the overall number ratio of W-R/O stars is ~ 0.05, i.e., normal compared to other regions in the Galaxy and the LMC.

8. The total intrinsic visual stellar luminosity from 30 Dor is only ~ 3 times greater than that for NGC 3603. However, NGC 3603, which emits more light from within $\phi = 0.5$ pc than does R136, is ~ 10 times smaller in linear extent (both in total breadth and in the core) and hence NGC 3603 is $\sim 10^3/3 \approx 300$ times denser, and more likely to be relaxed.

9. The ratio of total (ionized) gas mass to star mass appears to be ~ 17 times higher in 30 Dor than in NGC 3603. This may be the result of more efficient star formation especially at the low-mass end, in the higher metallicity Galactic region.

Subject headings: clusters: open — galaxies: Magellanic Clouds — nebulae: H II regions — nebulae: individual — stars: massive

I. INTRODUCTION

The true nature of the fuzzy cores R136 and HD 97950 of 30 Doradus and NGC 3603 respectively is still being debated. Either of the following possibilities for these prototypical, giant H II regions is of great interest: (*a*) a dense cluster core containing stars of normal masses ranging up to $\sim 100\ M_\odot$: Walborn (1973, 1984), Melnick (1982, 1983), Moffat and Seggewiss (1983), Huchra *et al.* (1983), and Walker and O'Donoghue (1984); or (*b*) a supermassive star (SMS) of mass $M \gtrsim 10^3\ M_\odot$ in the case of R136a, the brightest of three components within R136: Feitzinger *et al.* (1980); Cassinelli, Mathis, and Savage (1981); Ebbets and Conti (1982); Savage *et al.* (1983). More recently, Chu, Cassinelli, and Wolfire (1984) have claimed that the brightest unresolved component in R136a (i.e., R136a1) may be a single star with a mass of $\sim 750\ M_\odot$, or it may be a cluster of normal-mass O3 stars. However, before one accepts the consequences of either hypothesis (i.e., SMS or dense cluster core), an unambiguous decision should be attempted using the highest spatial resolution and best observing techniques possible from the ground.

The main conflicting interpretations so far come from:

1. Speckle interferometry (difficult for complex dense cores): Meaburn *et al.* (1982) claim just one bright central peak in R136a with a FWHM of $\sim 0\farcs2$ while Weigelt (1981; private communication) finds at least five components on a complex background. The old astrometric observations of van den Bos (Innes 1927), cf. also Moffat and Seggewiss (1983) and Worley (1984), favor the multicomponents of Weigelt.

2. Optical surface photometry: Moffat and Seggewiss (1983), using the photographically calibrated isophotes of Feitzinger *et al.* (1980) deduce $V \approx 12.1$ in the central seeing disk of R136, i.e., no brighter than the brightest resolved stars around R136. Chu (1984) and Chu, Cassinelli, and Wolfire (1984) find $V \approx 11.2$ for R136a1 (the brightest component in R136a) based on new photographic plates obtained in good seeing conditions (FWHM $\approx 1''$).

3. Ultraviolet (*IUE*) observations: Savage *et al.* (1983) note that in a region of $3''$ diameter centered on R136, the extinction-corrected UV/optical flux ratio is higher than usual for normal massive stars. However, as pointed out by Melnick (1983), this *IUE* diaphragm size refers to single star profiles and is only a rough guide for extended sources, as is the case for R136. Furthermore, based on the *IUE* response function (de Boor, Koornneef, and Meade 1981), the FWHM for a two-dimensional Gaussian fit is more like $\sim 5''$. In this case, the UV/optical flux ratio comes more in line with that from other normal massive stars.

Clearly, there is a need for superior quality data, e.g., CCD detector versus photographic plates and sky-subtracted spectra using small apertures. 30 Dor and NGC 3603 are the nearest examples of similar or even more massive giant and supergiant H II regions being studied in other, more distant galaxies, where spatial resolution is a much more serious problem. Hence, understanding 30 Dor and NGC 3603 may provide us with important clues to understanding extragalactic giant H II regions in general.

Many luminous, dense extragalactic H II regions show broad, Wolf-Rayet (W-R)–like emission lines, as do R136 and HD 97950 (Rosa 1983); the equivalent width of the $\lambda 4650 + \lambda 4686$ emission complex is typically diluted to ~ 10 Å. In this paper, we attempt to probe the stellar content of R136, HD 97950, and their surroundings. We emphasize the W-R component, as W-R stars are important probes of the most massive stars. Since W-R stars occur in relatively small numbers, they can easily be traced even in regions of relatively high star density. For a review of the stellar content of 30 Dor we refer to Melnick (1983) and Walborn (1984), and for NGC 3603 we refer to Moffat (1983*a*).

II. OBSERVATIONS

a) Spectrophotometry

During an interval of seven consecutive nights in 1982 December we obtained spectra using the image dissector scanner (IDS) sustem at the 1.5 m telescope of the European Southern Observatory, Chile, Twin diaphragms A, B of size $2'' \times 2''$ or $4'' \times 4''$ separated by $60''$ were employed. The seeing was typically $1''$–$2''$ FWHM. Integrations were normally made in series, with the source consecutively in ABBA and the background in BAAB. Total exposure times per series ranged from ~ 10 to ~ 40 minutes, depending on the source brightness. The spectral resolution (FWHM) was 3 Å in the blue (4000–5000 Å) and 6 Å in the red (5000–7000 Å). Pixel-dependent sensitivity was eliminated by exposure of a white screen illuminated by a quartz lamp in the dome (flat field). Flux calibrated from observations in the $4'' \times 4''$ aperture, only, of the standard stars Feige 15 and Hiltner 600. Wavelengths were established from a He-Ar line spectrum. The data were reduced using the image reduction software IHAP at ESO, Garching.

Spectra were obtained by visual centering for: (1) the central peak of R136a in $4'' \times 4''$ and $2'' \times 2''$ apertures each night in the blue and in $4'' \times 4''$ on two nights in the red, (2) a $6'' \times 6''$ mosaic of nine adjacent $2'' \times 2''$ positions centered on R136 in the blue on at least two nights each, (3) the nebula near R136 in the $2'' \times 2''$ aperture in the blue, (4) other W-R stars around

R136 for comparison (R136c, R134, R140b, R145, R130) in the 2″ × 2″ or the 4″ × 4″ aperture in the blue, (5) the central peak of HD 97950 in the 4″ × 4″ aperture each night in the blue and on two nights in the red, and (6) the components A, B, C, and D of HD 97950 in the 2″ × 2″ aperture in the blue on at least two nights each. Since A and B are separated by only 0″.6, the spectra labeled A and B will not be independent.

b) Imagery

During two nights in 1983 August we obtained CCD images at the f/2.67 prime focus of the 4 m telescope at Cerro Tololo, Chile. The unintensified CCD is an RCA thin-backed chip consisting of 500 × 312 pixels with separation 0″.60. The readout noise was ~50 electrons per pixel. The seeing was ~1″.3 FWHM, corresponding to an area of ~4 pixels. Images were obtained in each of three filters, whose characteristics in the f/2.67 beam are as follows: (*a*) broad band, centered at $\lambda = 4700$ Å with FWHM ~350 Å (to serve as reference continuum [+diluted emission] at the same central wavelength as the emission-line filters below); (*b*) narrow band, one centered at $\lambda = 4650$ Å and one at 4686 Å, both with FWHM ~35 Å (the former to detect C IV λ4650 in WC stars and, of secondary importance, N III λ4640 in WN stars; the latter to detect He II λ4686 in WN stars and, to a much lesser degree, in WC stars).

The results presented in this paper, based on the best image obtained with each filter, confirm the high rate of success attained by Wray and Corso (1972) using similar filters to distinguish WN and WC stars in M33 (cf. the spectrophotometry of Massey and Conti 1983).

Exposure times were 2–4 s in the broad-band filter and 12–40 s in the narrow-band filters such that the brightest part of the image (center of R136a or of HD 97950) was comfortably below staturation in all cases. Thus, following the experience of other users of this detector, we can assume linearity to better than 1% over the whole range of intensity in each image. Varying the exposure by a factor of 2 for 30 Dor yielded identical results.

Pixel-to-pixel sensitivity variations were eliminated by dividing each image by a flat-field image through each filter using a quartz lamp reflected from a white screen. Virtually all distortions above ~1%, including fringe effects, fully disappeared. Dark current was negligible. The bias level was determined by averaging ~50 frames of negligibly short exposure with the shutter closed.

Any mismatch in image structure between broad and narrow filter pairs (due, e.g., to seeing or focus differences) was compensated for by convolving the better image with a two-dimensional Gaussian function in order to yield the same profile for both pairs. Differences of ~10% mismatch in FWHM before the correction were encountered. Image pairs were also matched in X, Y by a translation (even by a small fraction of a pixel) of one image relative to the other.

III. DISCUSSION OF THE IMAGES

a) The Central Region of 30 Dor

i) *Detection of W-R Stars*

While Figure 1 (Plate 1) shows an overview of the 5′ × 3′ CCD field in the 4700 Å, wide filter, Figures 2 and 3 (Plates 2–5; part *a* in each has the same scale as Fig. 1; part *b* is a threefold enlargement of regions containing the most WN [Fig. 2*b*] and WC [Fig. 3*b*] stars) show the subtracted net images $N - kW$, after relative image translation, where N is the narrow band image at 4686 Å (Fig. 2) or 4650 Å (Fig. 3), and W is the broadband image. The constant k is chosen for each of Figures 2 and 3 so that the net image was zero in the mean for several bright known non–emission line stars, in particular for the stars R137 and R142, which are early B supergiants according to Walborn (1984); R138, which is AO I (Walborn 1984); and R141, which is B0.5 according to Feast, Thackeray, and Wesselink (1960).

The net He II λ4686 image of Figure 2 reveals the following information:

a) *All* known W-R stars stand out clearly, in addition to the two strong-line Of stars, Nos. 30 and 35N found by Melnick (1983).

b) only one new W-R/Of star is found, 15″ northeast of AB 11 in Figure 2*a*. Since the net emission is weak, this is likely to be an Of star if it is not a W-R + O binary. After completion of this paper Walborn (1985) obtained a spectrum of this star, and a preliminary determination of the spectral type is WN7-A.

c) while R136c is confirmed to be a W-R star, R136b is not (as noted by Chu, Cassinelli, and Wolfire 1984, but in contrast to Melnick 1983).

d) the fuzz around R136 (cf. Fig. 1) disappears, implying the presence of *a discrete number of W-R stars* superposed on an unresolved background of visually fainter non–emission line O and fainter stars (cf. Moffat and Seggewiss 1983).

e) the image at the position of R136*a* is elongated in the northeast-southwest direction (seen also in a second, independent image pair) and is larger than the corresponding image of a single W-R star. *This means that R136a consists of at least two W-R stars.*

f) regions of strong background nebulosity appear slightly negative as a result of nebular Hβ falling within (but at the edge of) the W filter but not in the N filter. This has no influence on the detection of pointlike W-R stars.

The net C IV λ4650 image in Figure 3 reveals the following information:

a) the strongest net stellar images by far are the two known WC stars Mk-E (WC5) and R140a (WN6 + WC5): cf. Phillips (1982) and Moffat *et al.* (1985). The latter is probably not a physical binary, but rather belongs to a compact group of three or four W-R stars (R140), possibly like the W-R stars in R136.

b) some WN stars also show up, especially those of late type (WN7/8), where N III emission dominates the 4650 Å filter. Nevertheless, the WC stars completely dominate over WN stars, as expected for the 4650 Å filter.

(*c*) R136a is very weak at λ4650, implying that it consists of WN stars of mean subtype ≤WN6.

From both net images, it is apparent that a CCD with the appropriate filters is an excellent combination to detect a complete sample of W-R stars (down to the strongest line Of stars), even in a complex background.

The plot of magnitude difference $m(N) - m(W)$ for $N = 4650$ versus 4686 Å in Figure 4 shows how W-R stars of different subclasses can be separated. This method is sensitive to *line equivalent width*, while direct image intensity subtaction $(N - kW)$ is sensitive to *line flux*. Single, strong-line WN stars tend to lie on a locus as expected on the basis of equivalent widths for N III λ4640 and He II λ4686, tabulated for galactic WN stars by Conti, Leep, and Perry (1983). While He II λ4686 changes little with WN subclass, N III increases from WNE through WN7, tapering off again (along with λ4686) at WN8.

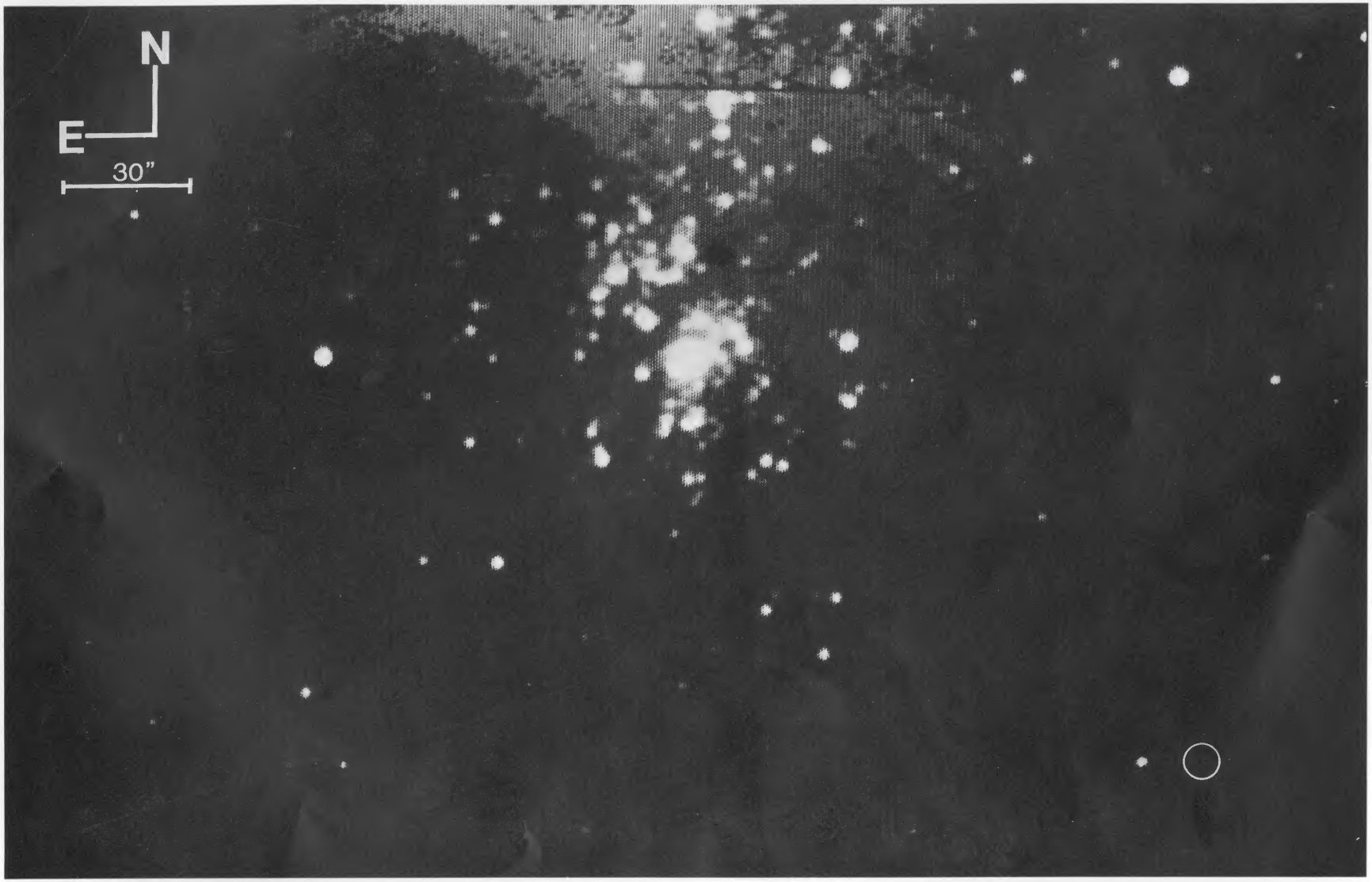

FIG. 1.—Overview of the 3′ × 5′ central CCD field of the 30 Dor region in the broad-band 4700 Å filter (FWHM = 350 Å). The circle has a diameter of 2 pc (7″.9)—compare with Fig. 10, in which the same intrinsic size circle has been drawn relative to HD 97950. This, as with other CCD images reproduced here, is a photograph of the video image display system.

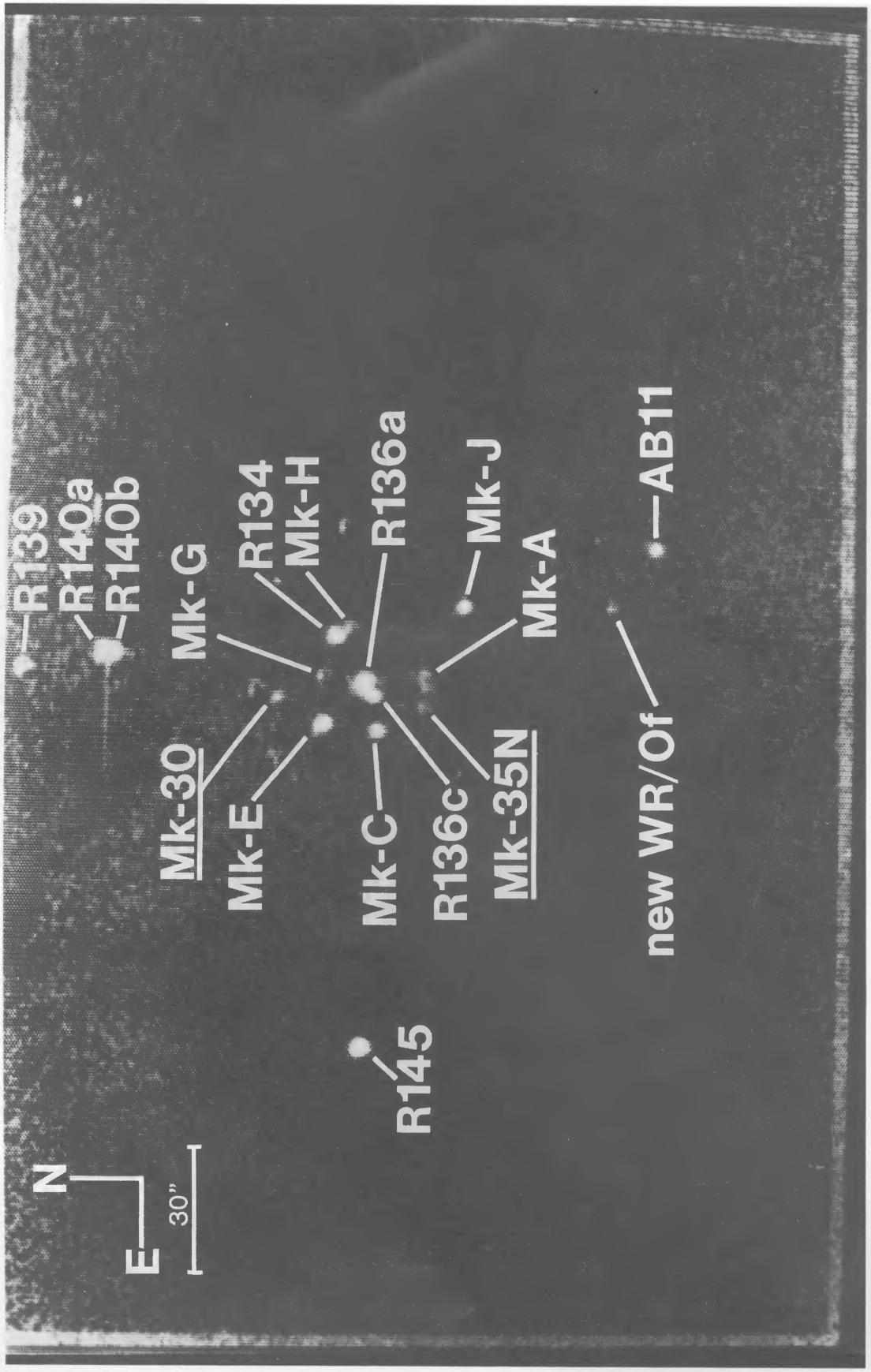

FIG. 2a

FIG. 2.—The net He II λ4686 CCD image ($N - kW$) for the central area of 30 Dor: (*a*) same scale as in Fig. 1, (*b*) a threefold enlargement centered on R136. All known W-R and strong-line Of (*underlined*) stars are identified (cf. Melnick 1982, 1983; Chu, Cassinelli, and Wolfire 1984) in addition to one new candidate near AB11. All other white patches are due to either noise or improper subtraction.

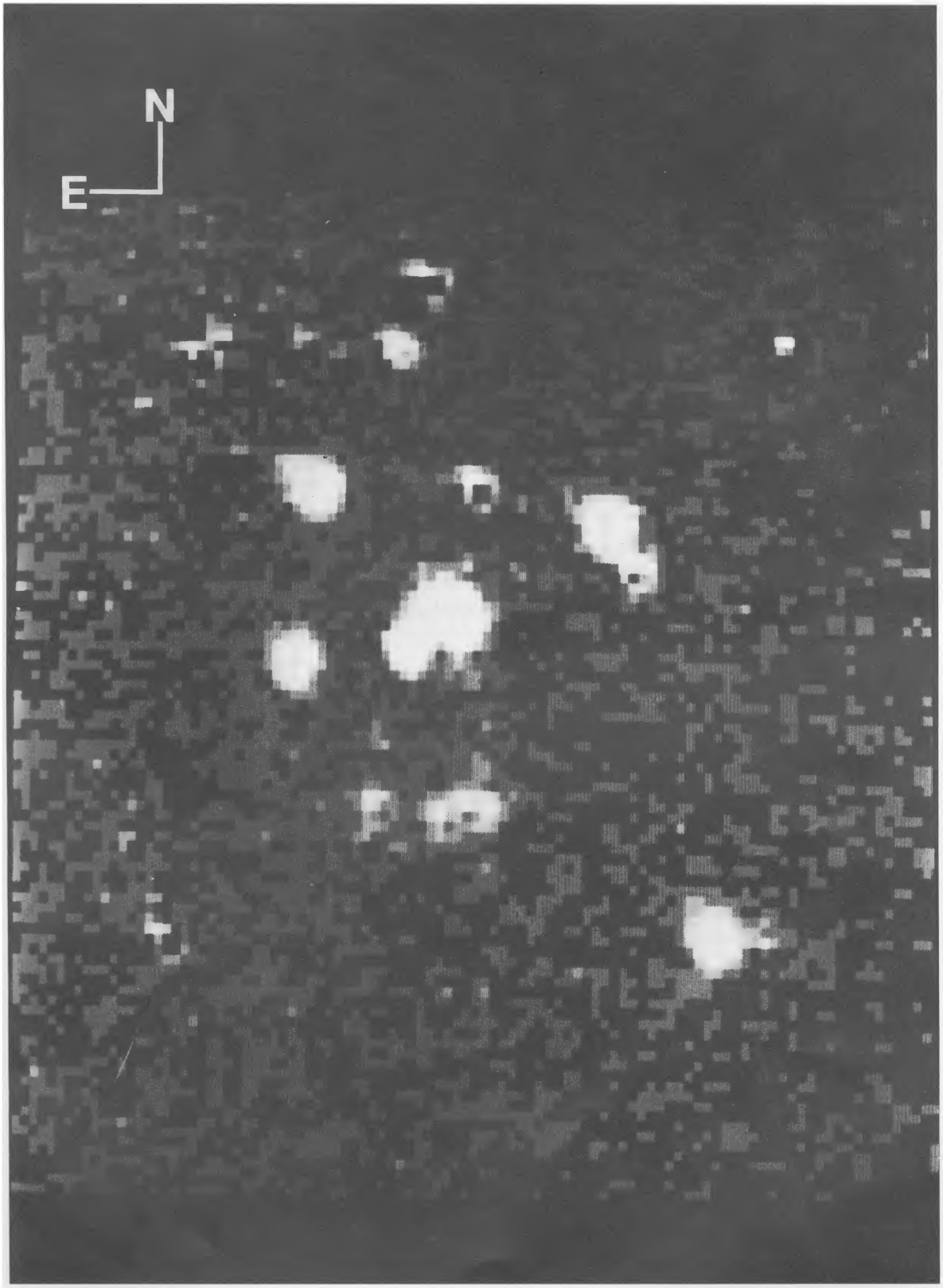

FIG. 2*b*

MOFFAT, SEGGEWISS, AND SHARA (*see* page 111)

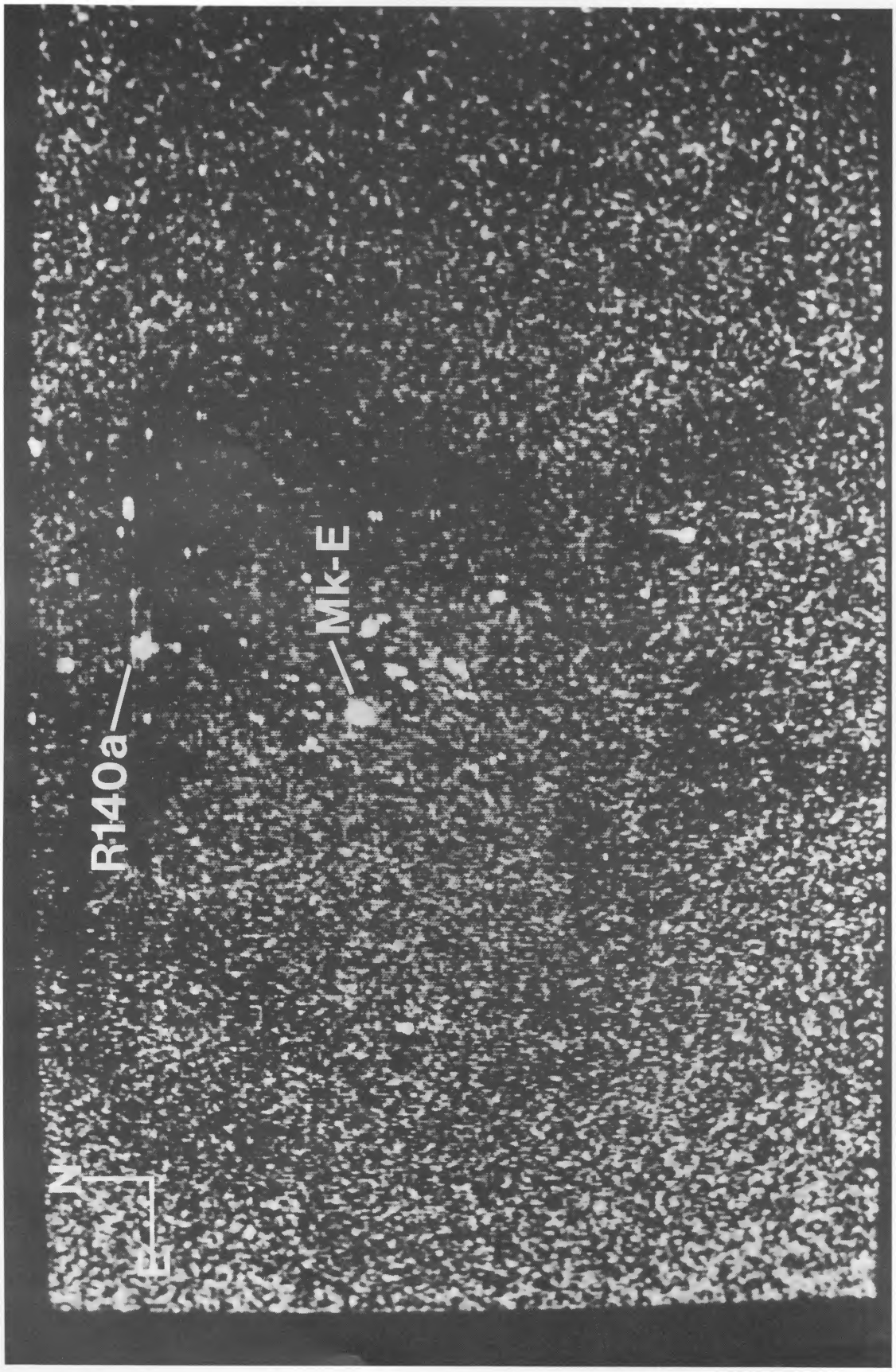

FIG. 3a

FIG. 3.—The net C IV λ4650 image ($N - k'W$) for the central area of 30 Dor: (*a*) same scale as Fig. 1, (*b*) a threefold enlargement to include the two strong-line WC stars.

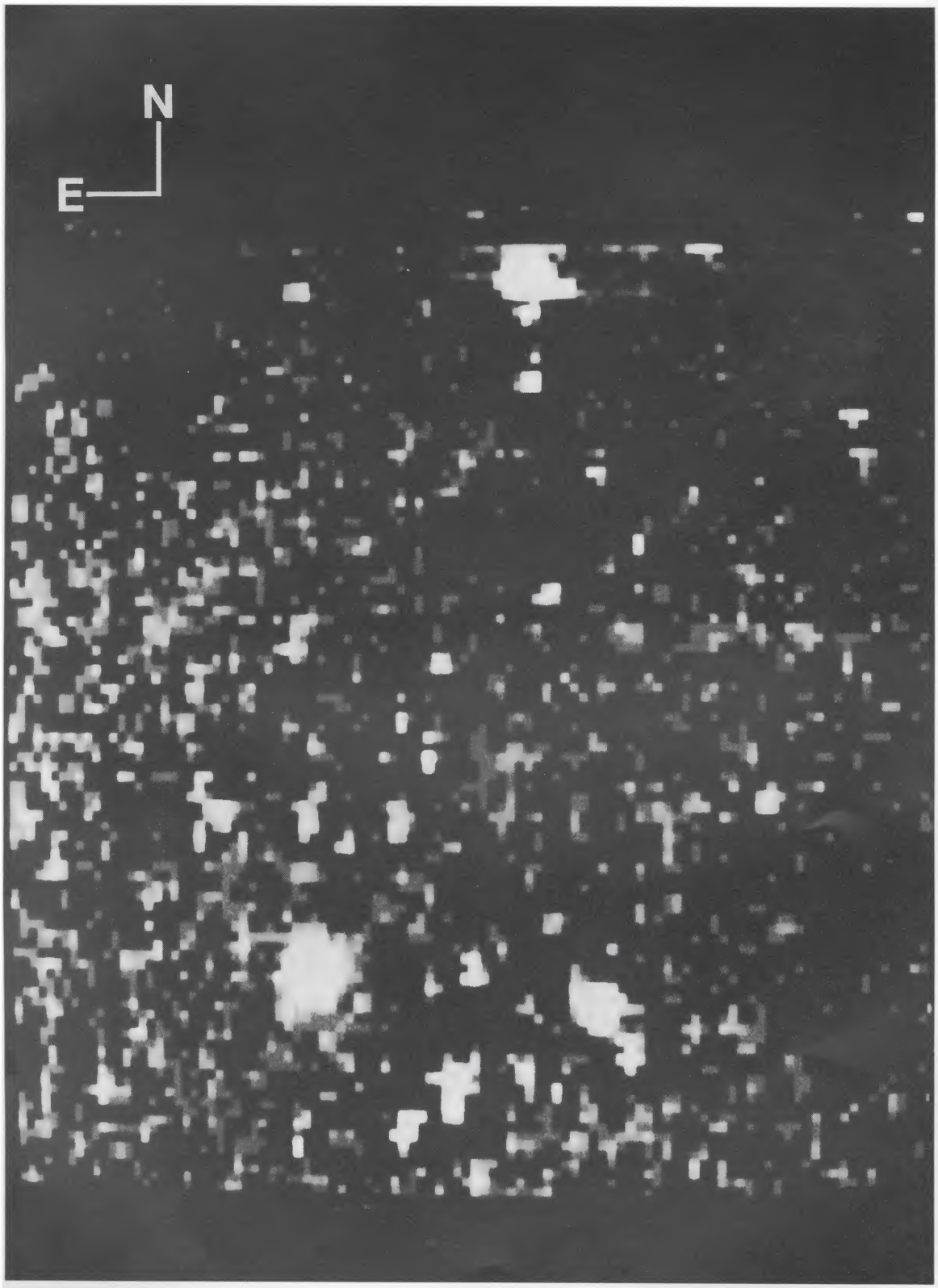

FIG. 3*b*

MOFFAT, SEGGEWISS, AND SHARA (*see* page 111)

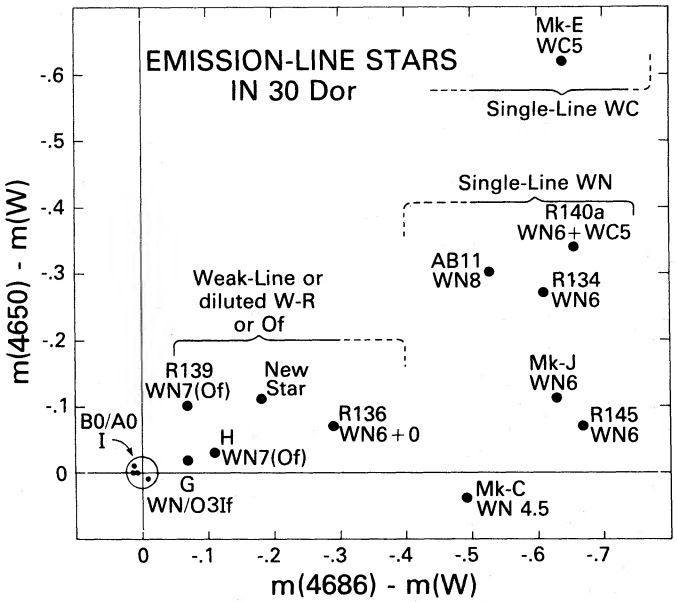

FIG. 4.—Magnitude differences $m(4650) - m(W)$ vs. $m(4686) - m(W)$ for relatively unblended stars. The differences are adjusted to zero for the four bright, early supergiants R137, 138, 141, and 142. Note the separation between WN (*lower*) and WC (*upper*), different WN subtypes and weak and strong line stars.

Note that the WN4.5 star has positive $m(\lambda 4650) - m(W)$ due to strong He II and very weak N III, so that the W filter contains relatively more emission than the 4650 Å filter. Furthermore, weal-line (in equivalent width, not necessarily line flux) stars lie low and to the left in Figure 4, as expected. These are Of stars or multiple W-R stars in which the emission lines are diluted by O star light, as is the case for R136a. Finally, WC stars tend to lie up to the right in Figure 4, although only WC5 stars are available in the sample. Note that the multiple type star R140a, WN6 + WC5, lies at an intermediate position.

Now we pass to the net emission images in the quantitative form of isophotes. Figures 5*a* and 5*b* show the net He II λ4686 isophotes in 30″ × 30″ regions around R136 and R140 respectively. The former shows that R136a is clearly elongated compared to single W-R stars (e.g., R134, Mk-E). This occurs mainly in a northeast-southwest direction, as noted above, and may be related to the brightest visual components in R136a, i.e., A and B (and others?) of Innes (1927). These two stars also lie along a northeast-southwest direction. Note also that the brightest stars in 30 Dor in general tend to be of type W-R (or, less frequently, B supergiants). We conclude, as before, that R136a contains *at least* two W-R stars.

The isophotes centered on R140 just north of R136 are also extended and asymmetric. This is not surprising, since R140 is a known multiple W-R system (with other stars?) with at least

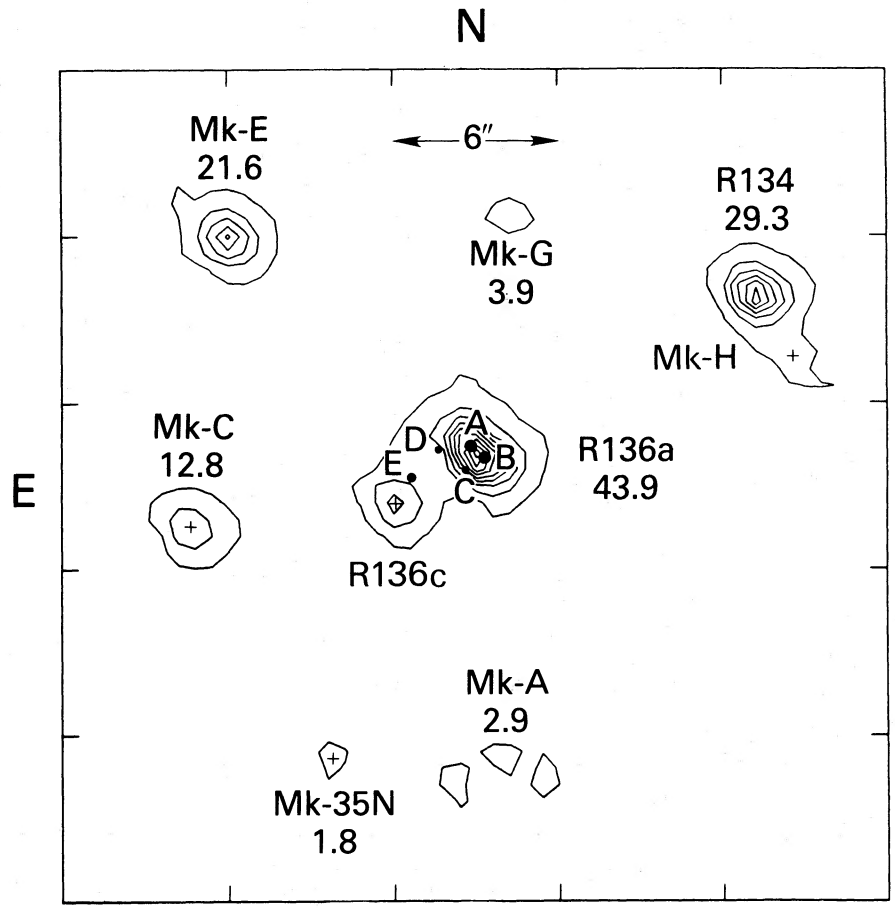

FIG. 5*a*

FIG. 5.—Linearly scaled isophotes of net He II λ4686 emission in a 30″ × 30″ region centered near (*a*) R136 and (*b*) R140. The maximum brightness (arbitrary units above a threshold of 1.5 above the background) is indicated for each detected emission-line stellar image. These agree well with the relative line strengths in the spectra of Fig. 19. The mean background is set to zero. Emission-line stars are identified as well as the multiple components in R136 of Innes (1927) with point size increasing with brightness. Innes' star E probably coincides with R136b, non–W-R.

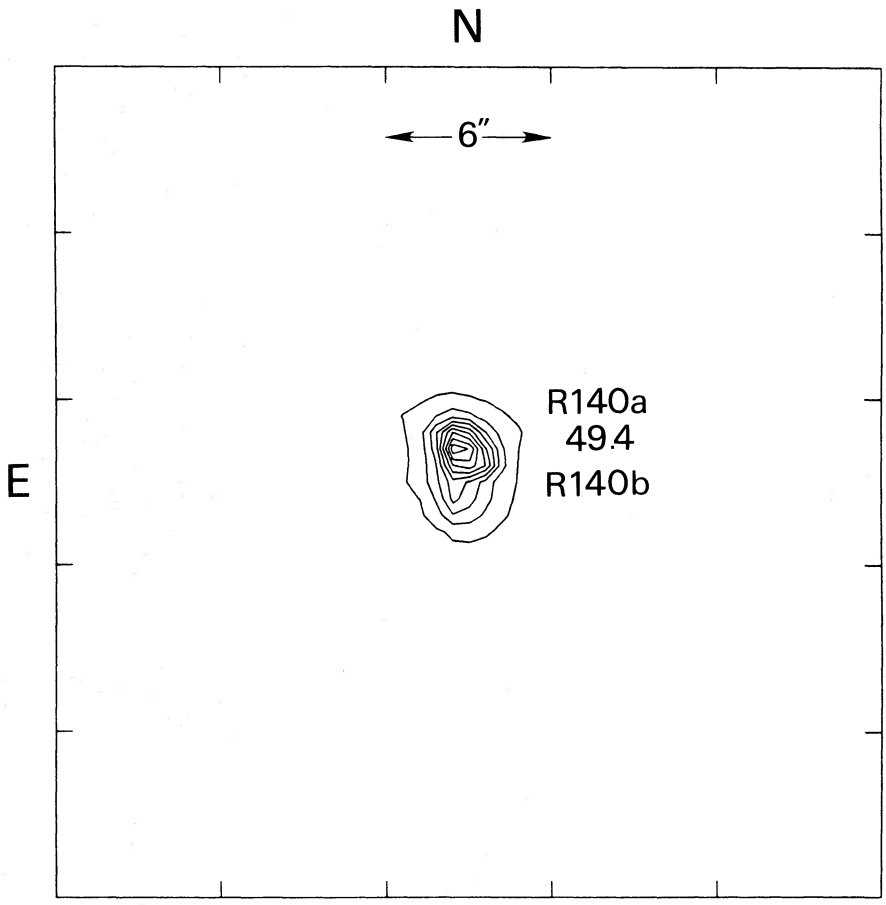

FIG. 5*b*

three distinct components (Moffat *et al.* 1985):

northern component { R140 a1: WN6 (SB1, +W-R?), R140 a2: WC5,

southern component R140 b: WN6: .

The northern and southern components are separated by $\sim 2''$. This means that R136 is not the only place in 30 Dor where several W-R stars exist, although R140 appears to lack the (stellar) fuzz of R136. This may be the distinguishing mark between a true cluster core (R136) at the geometrical center of 30 Dor and a knot of massive stars outside the center (R140). Note that the net He II λ4686 emission peak in R140 is only $\sim 10\%$ higher than in R136a. Allowing for the fact that the WC component in R140 has very strong lines, it is entirely possible that R136a consists of $\gtrsim 3$ W-R components.

Figure 6 shows the net C IV λ4650 isophotes in a $60'' \times 60''$ region including the two WC components, Mk-E and R140 a2. Both stars are of type WC5 and are discussed in relation to the overall population of W-R stars in 30 Dor by Moffat *et al.* (1985). *Note that at the position of R140, only one W-R star (the WC component) now shows up clearly, with a relatively symmetric profile compared to the net* He II *image in Figure 5b; the southern WN component has been almost perfectly subtracted out.*[4]

4 The east-west bulge in the isophotes of R140 is due to a bad column in the wide band image. A check on another independent image pair confirms the symmetric nature of R140 in λ4650 emission.

ii) *Radial Light Distribution*

We now investigate the radial distribution of light in the 30 Dor cluster, with origin centered on R136a—clearly the focal point of the cluster. We compare this distribution to that of a single star, R145 on the same image. This is done in the *W* filter ($\lambda = 4700$ Å), which is the filter least sensitive to W-R emission. Stellar magnitudes at λ4700 are not available. However, despite the differences in mean wavelength (4700 Å here versus 5500 Å in *V*) we can refer our data to integrated absolute *V* magnitude by shifting them to match the photoelectric *V* data for several different diaphragms (diameter $\geq 7''$) as tabulated from the literature by Moffat and Seggewiss (1983). The match is excellent at all radii.[5] We have assumed a true distance modulus $V_0 - M_v = 18.6$ and total visual extinction $A_v = 1.2$, to convert from apparent to absolute visual magnitude. This approach is justified by the facts that $E_{B-V} \approx$ constant (to ± 0.1 mag) for stars within the core region of 30 Dor (Fitzpatrick and Savage 1984), that photoelectric diaphragm photometry gives constant $B - V \approx 0.14$ from a radius of $3''.5$ to $30''$ from R136 (van den Bergh and Hagen 1968; Mendoza 1970; Feitzinger *et al.* 1980), and that the stellar content is similar everywhere on the average (Melnick 1983). The shift

5 The incorrect scale in Feitzinger *et al.*'s (1980) Fig. 6 (cf. Chu 1984; Chu, Cassinelli, and Wolfire 1984), from which Moffat and Seggewiss (1983) derived their magnitude–log radius relation within R136, has only a relatively minor effect, since the latter normalized to $V(\phi = 7'') = 10.0$ from photoelectric diaphragm photometry.

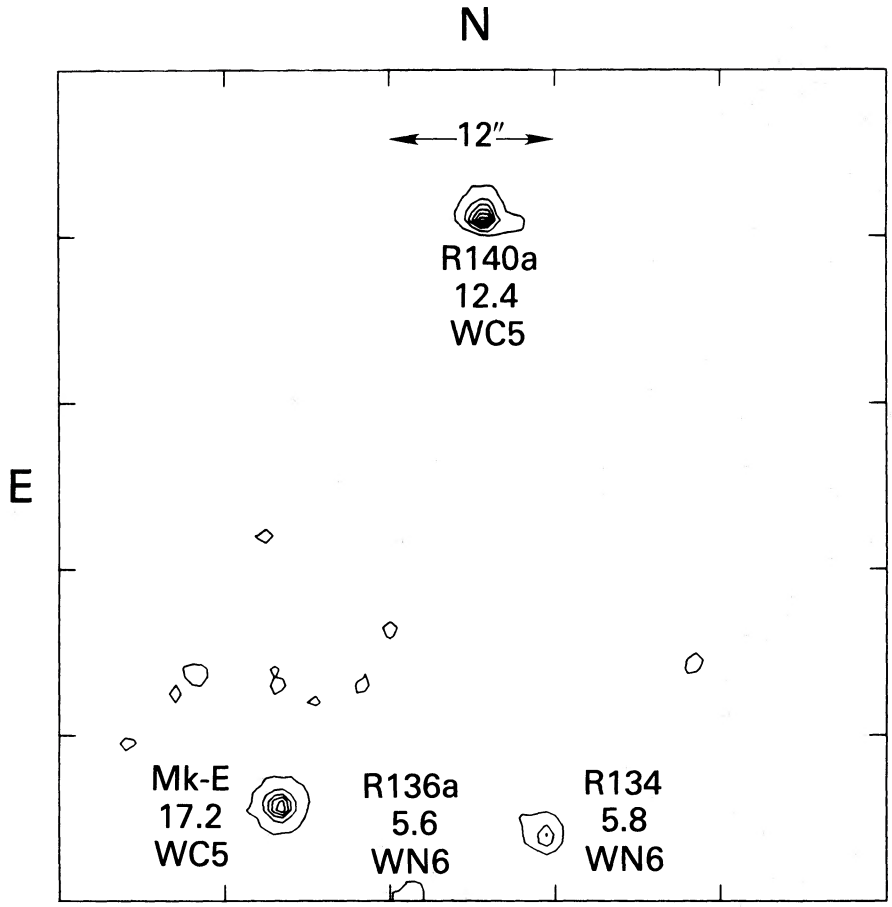

FIG. 6.—Linearly scaled isophotes of net λ4650 emission (C IV in WC, N III in WN stars) in a 60″ × 60″ region centered between R136 and R140. The mean background is set to zero. Emission-line stars are identified. Maximum surface brightness is not in the same units as in Fig. 5.

also yields the correct magnitude for R145 ($V = 12.0$, $M_v = -7.8$). Figure 7 shows the accumulative absolute and apparent visual magnitude as a function of radius r from R136a over about two orders of magnitude in r. The background level was chosen for two extreme limits (cf. Fig. 7): (*a*) low level, sampled near R145, and (*b*) high level, sampled between R136 and R138; the latter is probably more realistic in the mean, although the actual choice is unimportant in the central regions.

The observed core-halo structure of the 30 Dor cluster can be fitted well by a semiempirical isothermal King (1962) profile, valid for a variety of spherical stellar systems (neglecting tidal effects):

$$I(r) = I(0)/[1 + (r/r_c)^2] ,$$

where $I(r)$ is the observed surface brightness at projected distance r from the center, $I(0)$ is the central value of $I(r)$, and r_c is the so-called core radius. After integration of $I(r)$ out to successively larger radii, a fit to Figure 7 yields $r_c \approx 0.21$ pc (0″.82), reasonably similar to 0.32 pc obtained from independent but inhomogeneous data by Moffat and Seggewiss (1983). The fit is good at all radii to within $|\Delta M_v| \approx 0.1$ mag. The value of r_c lies just within the range observed among galactic globular clusters: $0.2 \lesssim r_c \lesssim 16$ pc (Peterson and King 1975). However, it is more appropriate to state that the true core radius in 30 Dor is ≤ 0.21 pc, since the derived value is less than a factor of 2 greater than the seeing radius ($\sigma = 0''.55$; see below). Mihalas and Binney (1981) on the basis of the work by Schweizer (1979) note that only values of r_c that satisfy $r_c/\sigma > 3$ can be considered reliable; otherwise the derived value should be taken as an upper limit. We draw attention to the fact that the lower resolution radio observations at $\lambda = 20$ cm of 30 Dor also show a core-halo structure, although on a larger scale (Mills, Turtle, and Watkinson 1978; Cersosimo and Loiseau 1984).

How bright is the unresolved, luminous stellar component at the center of R136? A first estimate of this is obtained by comparison of the radial surface brightness profile of R136 with that of the single star R145, in the same image (Fig. 7). The latter serves as the point-spread function (PSF). The profile of R145 has to be shifted vertically by 1.05 mag in order to match asymptotically the innermost data of R136. Since R145 has a mean magnitude $V = 12.01$ and color index $B - V = 0.11$, the latter being similar to that for R136 (Feitzinger and Isserstedt 1983), we derived $V = 12.0 - 1.05 = 10.95$ ($M_v = -8.85$) for the central unresolved core of R136, defined by the PSF. Referred to a star, *this magnitude is an upper (bright) limit, since it does not allow for any background light.* In an attempt to allow for background, we plot in Figure 8 (*bottom*) surface brightness versus radius for (1) the 30 Dor core, centered on R136a, and (2) R145. From this, it is clear that R136 is much

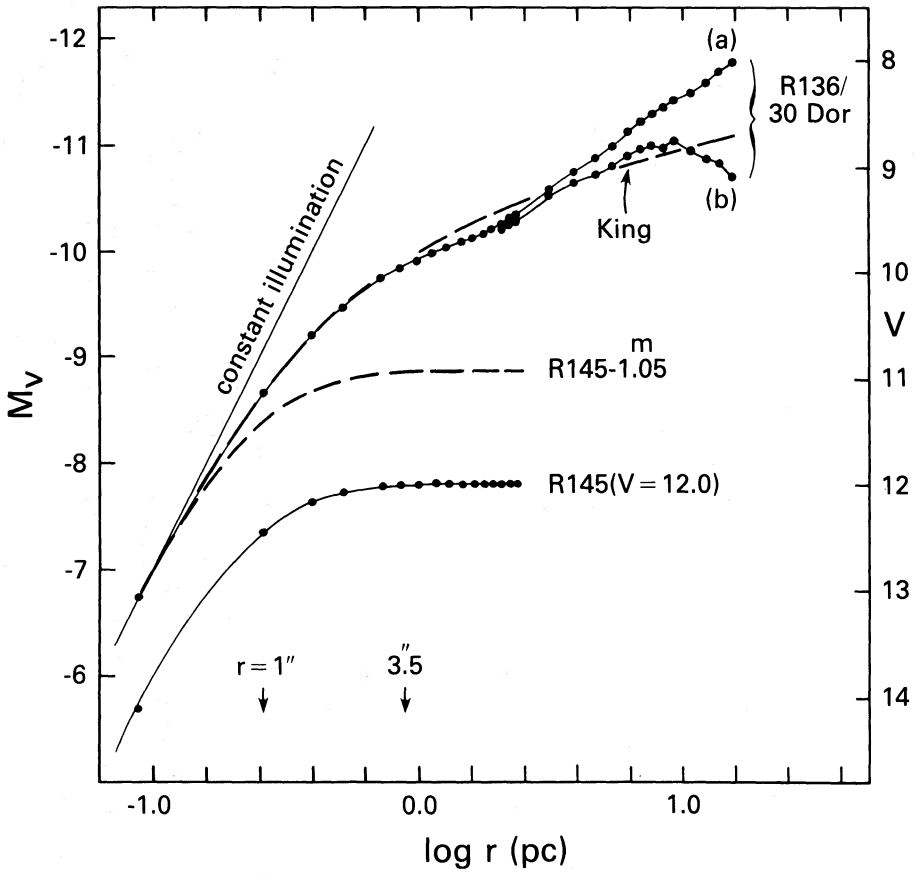

FIG. 7.—Accumulative absolute and apparent visual magnitude versus log radius (pc) from the broadband CCD image at $\lambda = 4700$ Å of 30 Dor centered on R136 (a = low background near R145; b = high background between R136 and R138) and centered on R145 (*solid curve*, observed; *dashed curve*, shifted 1.05 mag to match asymptotically the innermost part of R136). The dashed line through the R136/30 Dor data is a King profile fitted with $r_c = 0.26$ pc. The magnitude zero point was obtained by force fitting to photoelectric diaphragm V photometry from $r \approx 7''-\sim 20''$ from R136. Errors here and in other figures dealing with CCD brightness profiles are generally equal to or smaller than the size of the points plotted.

more extended than a single star.[6] Note that R145 gives a PSF with HWHM = 0.″66, which corresponds to a Gaussian core with $\sigma = 0.''55$. The PSF is well fitted by the empirical seeing profile (Moffat 1969):

$$f(r) = f(0)/[1 + (r/R)^2]^{\beta},$$

with $R = 1.''24$ and $\beta = 3.0$.

Taking the excess wings in R136 to be associated with the background light from unresolved stars whose numbers should increase with decreasing brightness, we can estimate the magnitude of the central unresolved star(s) in R136a as follows. In Figure 8 (*upper part*) we depict $I_{R136}(r) - kI_{R145}(r)$ versus r for different values of the constant k. The value of k can be constrained to $k \leq 1.8$ by assuming that there is in fact one or more bright unresolved star(s) at the center *and* that the background stellar light does not dip at the center. R145 is quite appropriate for this, since it has a W-R spectrum somewhat like that expected for the brightest stars within R136a. We thus find the magnitude of the unresolved stellar core of R136, after subtracting off the background core light, to be $V = V_{R145} - 2.5 \log k \geq 11.4$, corresponding to $M_v \geq -8.4$ if $V_0 - M_v = 18.6$ and $A_v = 1.2$ (Savage *et al.* 1983). *This is only ≤ 1.4 times brighter than the brightest resolved star outside but near R136, R144*—itself a *single* W-R star of type WN6 (Moffat 1985). R144 is one of the brightest stars in 30 Dor—there is no doubt that it is a member of the same complex as R136.[7]

If, as is likely, this central object of R136a is composed of more than one star (e.g., components A and B of Innes 1927, or the three resolved central speckle components in $\phi = 0.''5$ of Weigelt 1981), then the individual magnitudes will be even fainter. This reinforces the claim of Moffat and Seggewiss (1983), based on inferior quality data, that *R136 does not contain extraordinarily bright stars.* Note that based on photographic images Chu, Cassinelli, and Wolfire (1984) derive $V = 11.2$ for the brightest unresolved central star, R136a1.

[6] One might suspect this to be due to the dominating influence of the bright nearby components R136b and R136c. However, the smeared-out surface brightness in a ring one pixel wide at $r = 2.''1$ (R136b) and $r = 3.''4$ (R136c) from R136a, amounts to $\lesssim 8\%$ of the observed radial surface brightness for R136b and $\lesssim 12\%$ for R136c. Hence, we consider these two components merely as small perturbations to a generally smooth and slow drop in surface brightness of the fuzz in R136 as one proceeds to larger radii.

[7] Note that with $V = 11.2$, R144 is *apparently* much brighter than R145, with $V = 12.0$; however, with $B-V = -0.1$, R144 suffers less extinction than R145 ($B-V = +0.1$) and is intrinsically only slightly ($\Delta M_v \approx 0.2$ mag) brighter than R145. As opposed to R144, R145 is a single-line spectroscopic binary with a normal mass function (Moffat 1985).

In *absolute* terms, all the above M_v values will be made 0.4 mag fainter if the distance modulus of the LMC is 18.2, based on cluster main-sequence fitting by Schommer, Olszewski, and Aaronson (1984), instead of 18.6 adopted here. This lower distance brings the *mean* M_v of the WN6/7 and WN + O/Of stars of 30 Dor more in line with the mean M_v of similar galactic objects (Moffat *et al.* 1985).

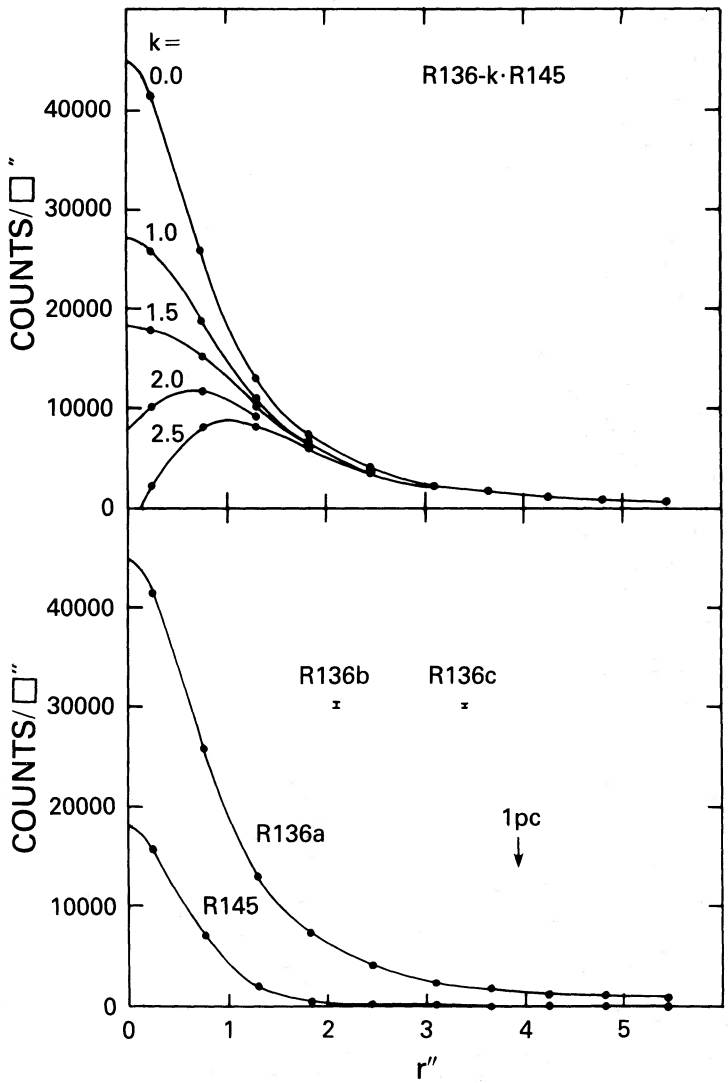

FIG. 8.—(*bottom*) Radial surface brightness (CCD counts arcsec^{-2}) vs. the radius from the center of R136a and R145 in the broad 4700 Å filter. The curve through the R136 data is a hand-drawn fit, while that through the R145 data is a fit to the empirical seeing profile of Moffat (1969) with $R = 1''.24$ and $\beta = 3.0$. (*top*) Net surface brightness $I_{R136}(r) - kI_{R145}(r)$ for different values of the constant k. The contributions of R136b and R136c are indicated by vertical bars.

Walker and O'Donoghue (1984) obtain $V = 11.45$ ($M_v = -8.3$) from broad-band CCD images.

Furthermore, as similarly noted by Moffat and Seggewiss (1983), R136 emits $M_v = -9.85$ from within the generous dimension of $\phi = 7''$, compared to a total of $M_v \lesssim -11.2$ in 30 Dor (limit within $\phi = 2'$, where the bulk of the hot stars in 30 Dor lie). This difference of $\gtrsim 1.35$ mag means that R136 provides $\lesssim \frac{1}{4}$ of the total visual output from stars in 30 Dor. This fraction drops even more, to $\lesssim \frac{1}{7}$, if one restricts the calculation to R136a alone in $\phi = 3''$, say.

In the UV, the situation is similar. From Figure 2 of Koornneef and Mathis (1981), one can easily derive, on the basis of the minor diaphragm dimension of 10″,

$$\frac{L_{UV}(\phi = 10'')}{L_{UV}(\phi = 2')} \approx \frac{1}{6},$$

or even less if one were to take a smaller diaphragm for R136. Similarly, Huchra *et al.* (1983) estimate that R136 ($\phi = 3''$) radiates ~10% of the total stellar UV light in 30 Dor. A reasonable overall estimate is that *R136 radiates ~20% of the total light from 30 Dor*, from stars of similar type to those in the surroundings of R136. This is in contrast to statements found in the literature that R136 provides most of the energy output to ionize the 30 Dor nebula. It should be noted that the projected number density of W-R stars plotted radially from R136 also satisfies a King profile out to $r \approx 100$ pc, i.e., ~5 times further out than the surface brightness didstribution in Figure 7 (cf. Moffat *et al.* 1985). Unfortunately, this number density distribution cannot be used to confine the core radius r_c.

We finally turn to the radial distribution of accumulative surface brightness in net He II λ4686 emission. This is shown centered on R136a and R145, respectively, in Figure 9. We note that the profile of R136 asymptotically approaches that of R145 at the center, after a shift of ~0.30 mag (factor of 1.3). This means that, at its center, R136 is ~$\frac{1}{4}$ fainter in λ4686 emission than R145. Allowing for differences both in line shape (cf. Fig. 19) and in the filter transmission curve, the actual λ4686 line flux is more nearly the same in both. However, as in the case of the distribution in broad-band light, R136 in emis-

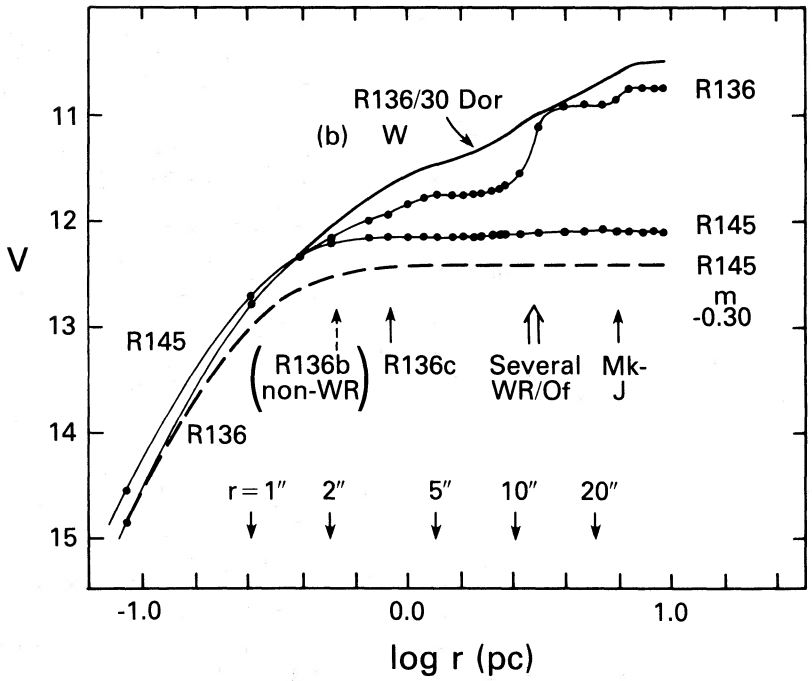

FIG. 9.—Accumulative radial brightness distribution in magnitudes, with the same zero point as in Fig. 7, of the net He II λ4686 emission centered on R136a and R145. Shifting R145 downwards by 0.30 mag (factor of 1.3), makes their central surface brightnesses coincide. The profile of the wide-band image of R136/30 Dor with high background subtracted is shown for comparison; it has been shifted in magnitude to match the inner region of R136 in net He II emission.

sion is clearly more extended than the astrometrically single WN6 star R145, even within $r \lesssim 2''$ of its center. Since the next closest W-R star, R136c, is at $r = 3''.4$ (R136b is non–W-R; see also Chu, Cassinelli, and Wolfire 1984), this implies that R136a contains *at least* two W-R stars, as already presumed on the basis of the non-symmetric isophotes in Figure 5*a*. Together, the W-R stars in R136a emit about as much λ4686 emission as R145 alone. This is not too surprising, since R145 is a relatively strong narrow-line W-R star. Presumably, the ≥ 2 W-R stars in R136a are of average line strength, possibly more like R134. Beyond $r = 2''.7$, R136c makes R136 noticeably more intense than R145 in net He II emission. The next known W-R star is located at $r = 9''$ from R136a.

The overall distribution of net λ4686 emission in the core of 30 Dor out to $\phi \approx 1'$ resembles the distribution of continuous light. This is not surprising, as the relative fraction of W-R stars appears to be nearly constant throughout the region (cf. § IV).

b) The Central Region of NGC 3603

i) *Detection of W-R Stars*

As in the case of 30 Dor, we consider the CCD images of NGC 3603 in the wide filter directly in Figure 10 (Plate 6), and in net He II λ4686 emission ($N - kW$) in Figure 11 (Plates 7–8). The factor k is found again by nulling bright non–W-R stars. The net λ4650 emission image provides no new information, other than to show that there are no WC stars in the $3' \times 5'$ central area of NGC 3603. The net λ4650 image is fainter than, but otherwise similar to, the net λ4686 image, since the WN type N III λ4640 emission which falls in the 4650 Å filter is weaker than He II λ4686.

The only W-R stars seen in the $3' \times 5'$ central region are WN stars located in the core, HD 97950. The O6 If star Sher 18 (cf. Moffat 1983*a*), is only marginally visible in net emission. Again, as with 30 Dor, the nebular subtraction is not perfect due to Hβ emission in the wide filter; however, this also has no effect here on the interpretation. The unresolved background fuzz around HD 97950 also disappears in the net emission image as in the case of R136. This light must arise in non–W-R stars, mostly of O type.

Figure 12 shows the isophote plot in net λ4686 emission in a $12'' \times 12''$ area around HD 97950. The positions of the astrometric visual components of van den Bos (1928) are shown superposed on the linearly scaled isophotes. Since there are no other W-R stars in the $3' \times 5'$ field for comparison, we consider the isophotes of a single, bright star (Sher 1965 No. 3, a foreground B star) located within the field. These are shown in Figure 13 for both wide and narrow images, before subtraction (after subtraction, this star completely disappears). Each of these profiles is perfectly round to within ~5%, while the λ4686 image of HD 97950 in Figure 12 is elongated by ~35% in a direction defined by the relative positions of components A, B, and C. We estimate that HD 97950 contains at least two W-R stars and probably contains three (in each of A, B, and C). More details are given in a separate spectroscopic study of HD 97950 by Moffat and Niemela (1984).

ii) *Radial Light Distribution*

As with 30 Dor, we now pass to the radial distribution of light in the cluster NGC 3603, with origin centered on HD 97950 AB. This is compared to a single star, Sher No. 3 ($V = 11.03$, $B-V = +0.19$ according to Sher 1965), on the same image. With $V_0 - M_v = 14.2$ (7 kpc) and total visual extinction $A_v = 4.4$, being nearly constant for all cluster members (Moffat 1983*a*), we easily convert our λ4700 magnitudes to absolute visual magnitude M_v by applying the same shift procedure as in the case of 30 Dor. The match between the photoelectric V photometry in different diaphragms (cf. Moffat and Seggewiss 1983) and the present λ4700 values after shifting

PLATE 6

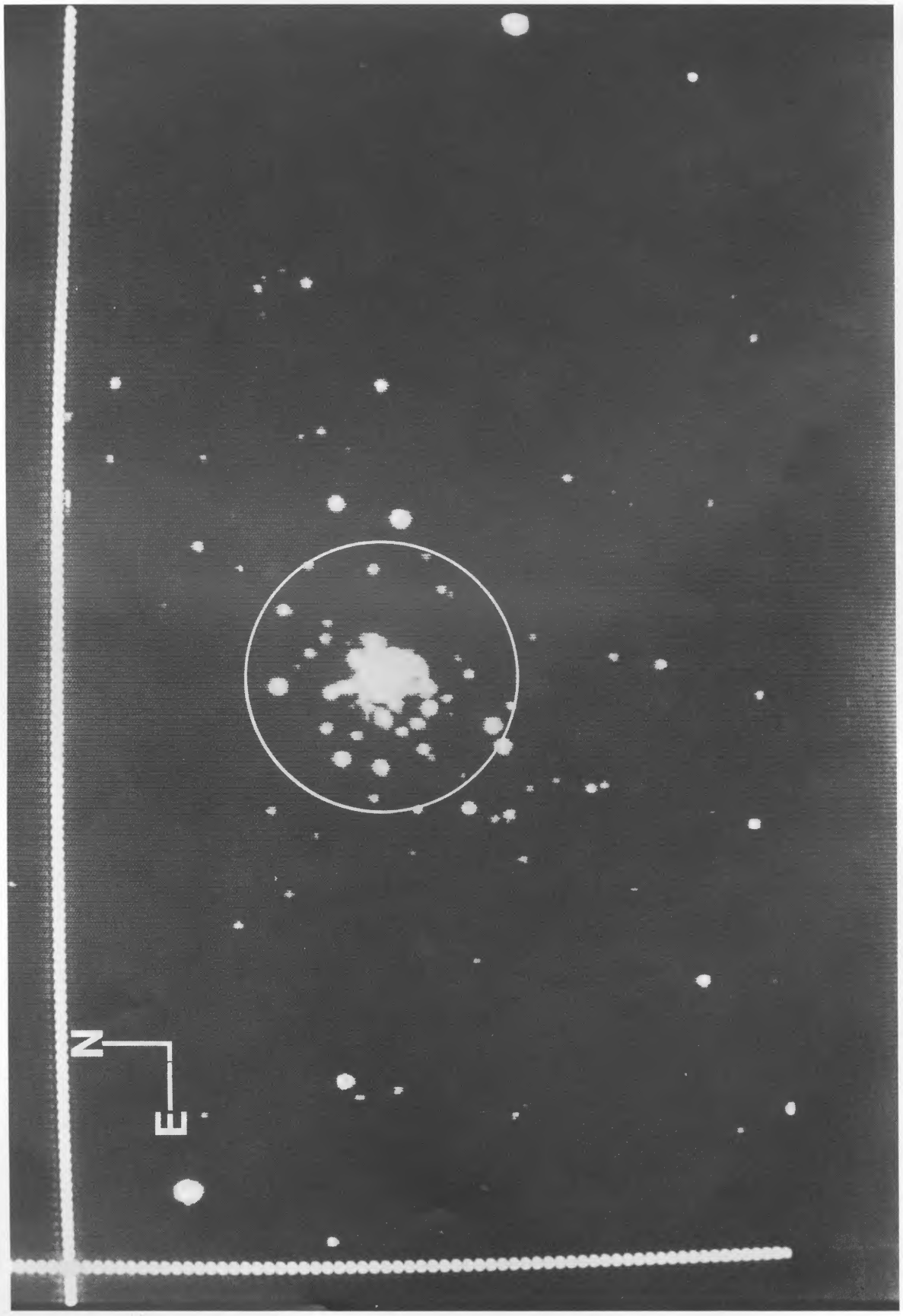

FIG. 10.—Overview of the 5′ × 3′ central field of NGC 3603 in the broadband 4700 Å filter. The circle has a diameter of 2 pc (59″).

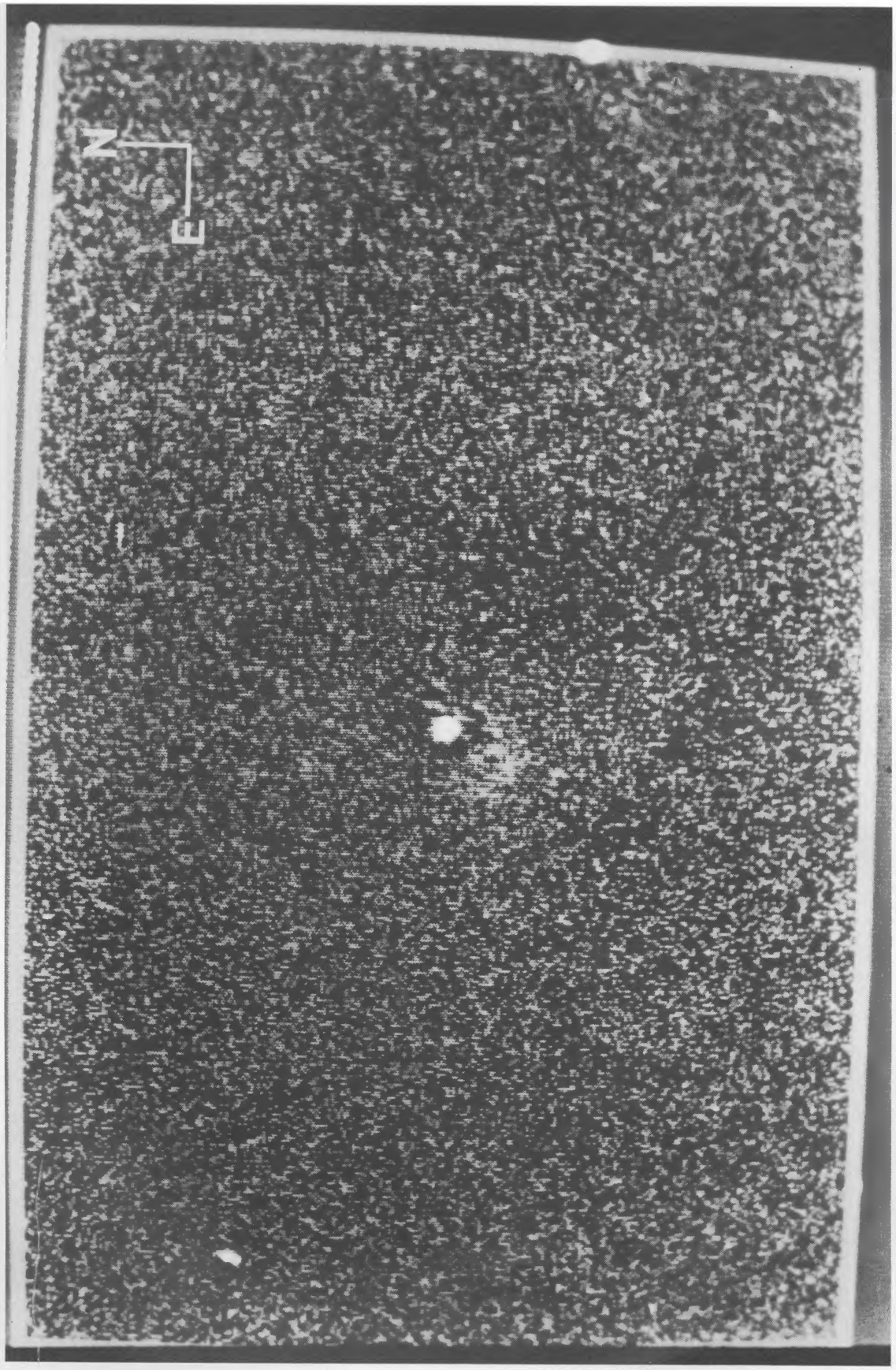

FIG. 11*a*

FIG. 11.—The net He II 4686 CCD image ($N - kW$) for the central area of NGC 3603: (*a*) same scale as Fig. 10, (*b*) a threefold enlargement centered on HD 97950, the bright object at the center. The O6 If star Sher No. 18 is identified.

PLATE 8

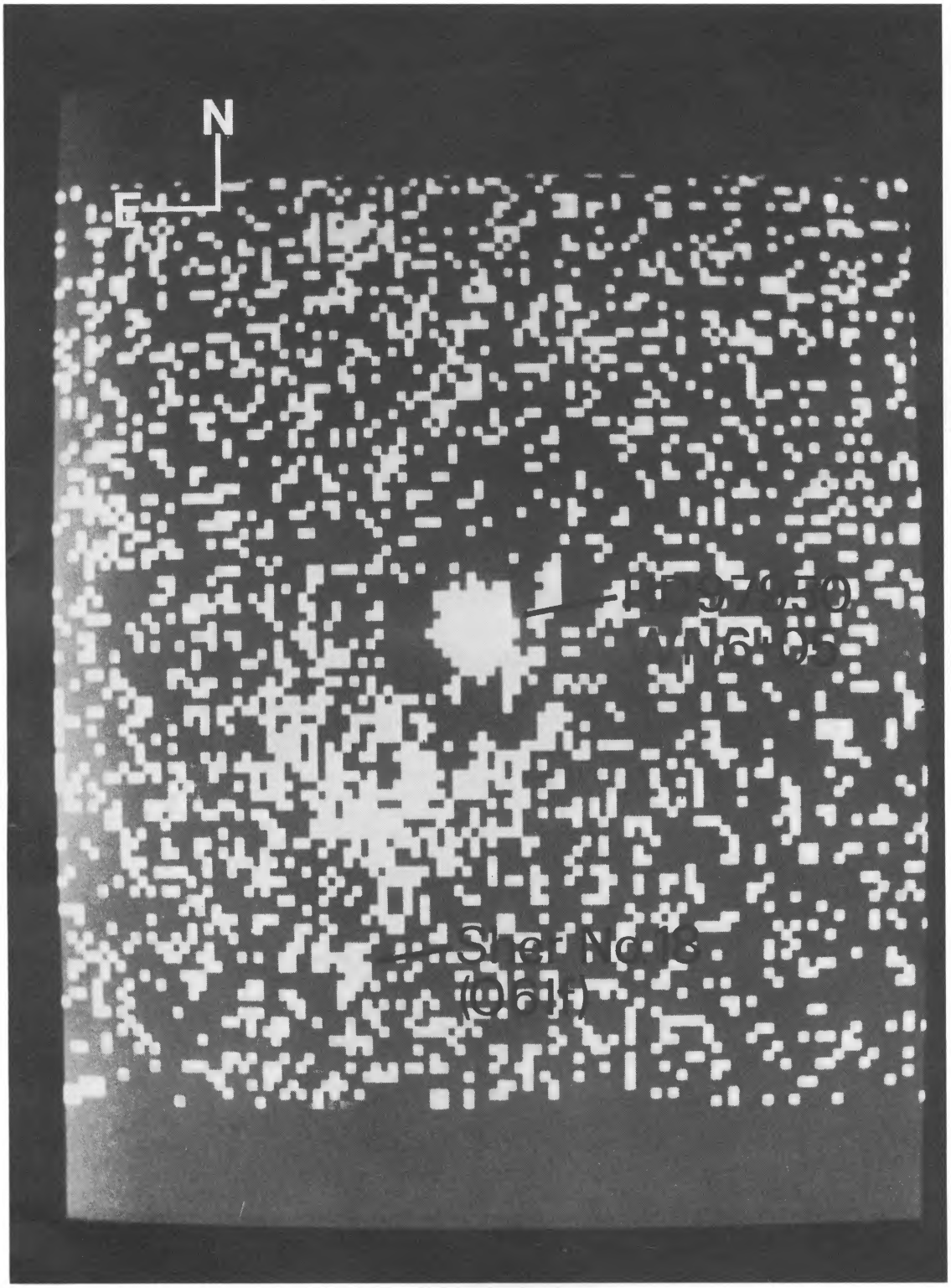

FIG. 11*b*

MOFFAT, SEGGEWISS, AND SHARA (*see* page 117)

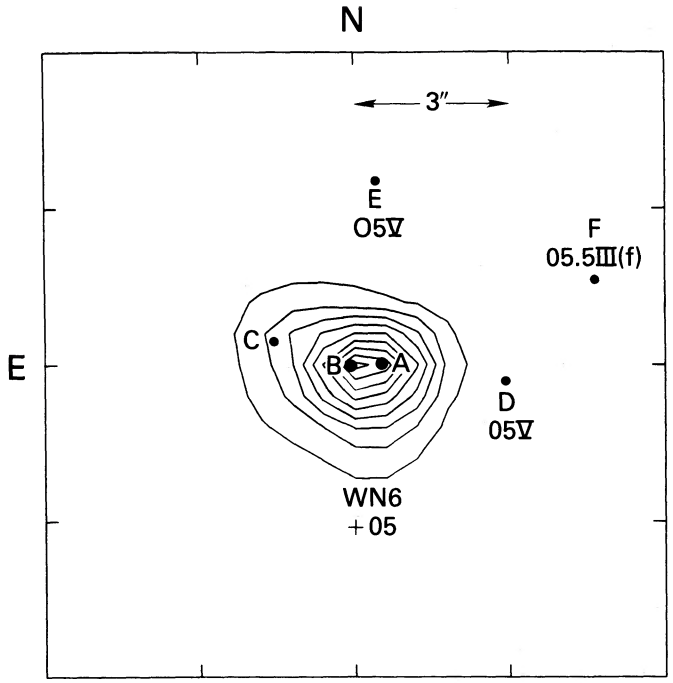

FIG. 12.—Linearly scaled isophotes of net He II λ4686 emission in a 12″ × 12″ region centered near HD 97950. The mean background is set to zero. The multiple components of van den Bos (1928) are identified, with point size increasing with brightness.

is excellent. It should be noted, however, that overlap is limited to the range $r = 2\farcs5$–15″. Figure 14 shows the accumulative absolute visual magnitude as a function of radius from HD 97950 AB. The radii range over about two orders of magnitude. The background nebula is much less intense on our short-exposure images than in 30 Dor; hence *where* it is sampled in a starfree region is virtually irrelevant.

In Figure 14 we fit a King profile to the accumulative magnitude versus log radius. The fit is even better than for 30 Dor ($|\Delta M_v| < 0.1$ mag) over two decades in r. We obtain a core radius $r_c \approx 0.024$ pc ($0\farcs71$), similar to 0.030 pc obtained previously (Moffat and Seggewiss 1983). This core radius is well below the normal range for galactic clusters. We note again that the true core radius, if it is nonzero, may be significantly less even than this, since it is very close to the Gaussian seeing radius ($\sigma = 0\farcs55$ here). In any case, taken at face value, the core radius of NGC 3603 is ~10 times smaller than that of 30 Dor. The fact that the outer extent of NGC 3603 is also a factor of ~10 smaller than the 30 Dor cluster suggests that the galactic object represents a geometrically scaled down version of the giant 30 Dor Nebula.

By comparing with Sher No. 3 in Figure 14, the asymptotic magnitude of a central, unresolved star (or stars) in HD 97950 is $M_v \gtrsim -8.15$, compared to $M_v \gtrsim -8.85$ (-8.45 for $V_0 - M_v = 18.2$) in R136. Neither of these estimates allows for background light. However, within a fixed *linear* radius of 0.5 pc, say, ($\phi = 1.0$ pc, corresponding to $3\farcs9$ in R136 and 30″ in NGC 3603, i.e., easily resolved in both) we find $M_v = -9.6$ in NGC 3603 and $M_v = -9.4$ (-9.0 for $V_0 - M_v = 18.2$) in R136. This means that NGC 3603 is intrinsically brighter than R136 on this scale; the difference becomes even more pronounced at smaller diameters. Hence, if star density is proportional to light output, this implies that *NGC 3603 is denser than the core of 30 Dor* within the same external radius ≤ 0.5 pc.

As in the case of R136, the central core of NGC 3603 can be decomposed into an unresolved, bright star or group of stars (e.g., components A, B in our $1\farcs3$ FWHM seeing) and background stellar light, which should also peak or at most flatten out at the center. In Figure 15 (*bottom*) it is apparent that HD 97950 is more extended than a single star. Calculation of $I_{\rm HD\,97950}(r) - kI_{\rm Sher\,No.\,3}(r)$ for different values of the constant k shows that $k \leq 0.9$ to avoid a dip in the background at the center (cf. Fig. 15 [*top*]). We thus find a net magnitude for the unresolved core of HD 97950: $M_v = -8.10 - 2.5 \log k \geq$

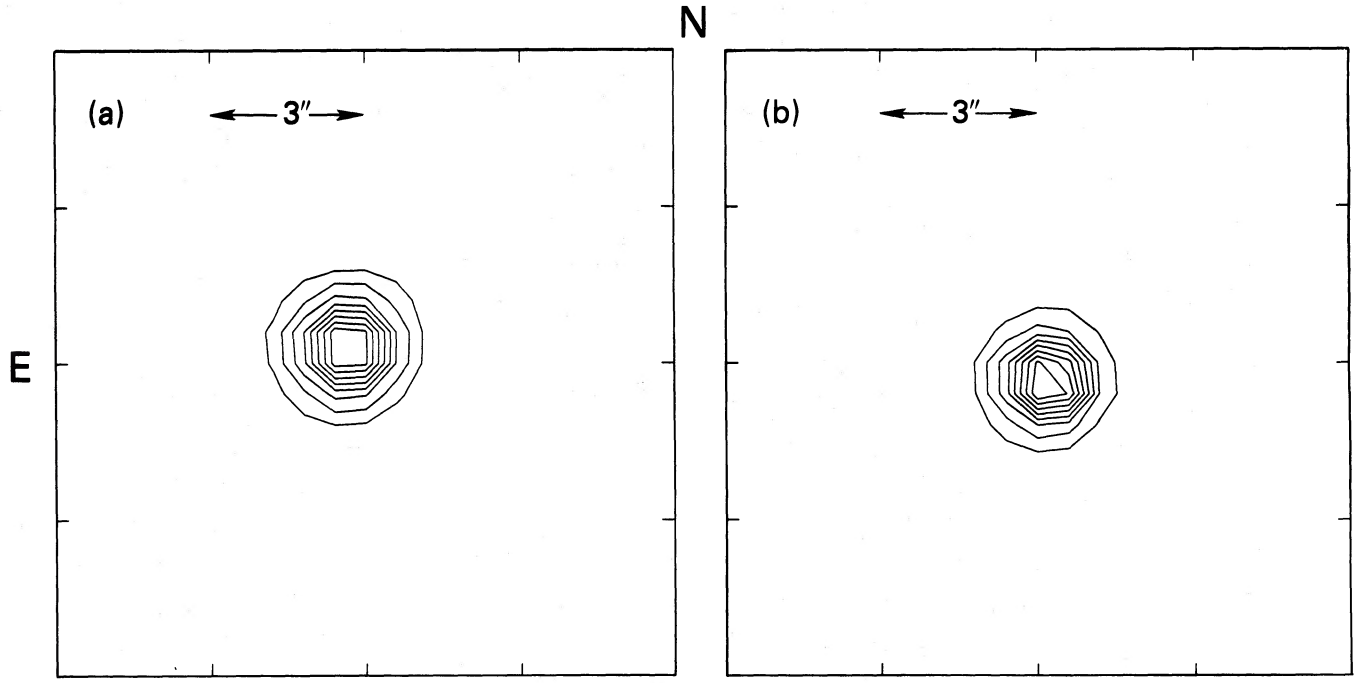

FIG. 13.—Linearly scaled isophotes of a 12″ × 12″ field centered on the field B star Sher No. 3 in (*a*) narrow-band λ4686 and (*b*) wide-band λ4700.

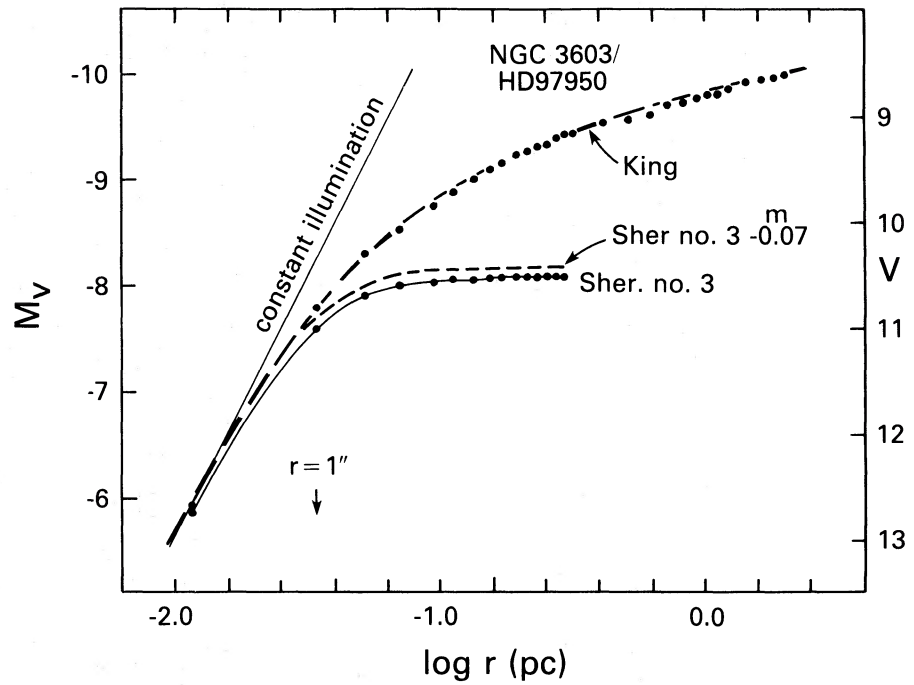

FIG. 14.—Accumulative absolute and apparent visual magnitude vs. log radius (pc) from the broad-band CCD image at λ4700 of NGC 3603, centered on HD 97950AB and on Sher No. 3 (*solid curve*, observed; *dashed curve*, shifted 0.07 mag to match asymptotically the innermost part of NGC 3603). The dashed line through the HD 97950/NGC 3603 data is a King profile fitted with $r_c = 0.024$ pc. The V magnitude zero point was obtained by force fitting to photoelectric diaphragm V photometry centered on HD 97950. Hence, the V magnitude of Sher No. 3 does not correspond to its published value.

-8.0, assuming $V_0 - M_v = 14.2$ and $A_v = 4.4$. Since this probably refers to the nearly equal components A and B (themselves each possibly multiple; Baier, Ladeback, and Weigelt (1985) find component A to be triple and B single at 0".09 resolution), each of these components would have $M_v \gtrsim -7.25$, in the range of *single* galactic WNL stars.

Finally, we look at the radial distribution of net λ4686 emission in HD 97950 in Figure 16. This confirms our impression based on the isophotes in Figure 12 that the λ4686 emission from HD 97950 is clearly extended. We similarly conclude that NGC 3603 contains at least two, if not three, W-R stars confined to within the dense central area defined by HD 97950 A, B, C. The O6 If star Sher No. 18 probably causes a rise in the curve at its corresponding distance from the center of HD 97950. Note that the radial distribution of λ4686 emission behaves much like that of the continuum light within $r \approx 2''$ of the center. Whether we are dealing with small numbers or whether relaxation has caused the most massive stars (i.e., W-R progenitors) to settle into the cluster core is a question which we address below.

IV. DISCUSSION OF THE SPECTRA

a) The 30 Dor Core

We first searched for gross line variations by comparing the spectra from each of the seven nights. No significant profile variations were seen, either in the 2" × 2" or the 4" × 4" apertures centered on R136a.

Next, we looked for variability of line position, i.e., radial velocity (RV). Table 1 lists the RVs of the two strongest emission lines as a function of time, i.e., He II λ4686 from the W-R component (N IV λ4058 is too weak to be useful) and [O III] λ5007 from the nebula. The 4" × 4" aperture data should be more reliable because the wavelength calibration was only carried out in 4" × 4", and it was more difficult to center R136a the same way each night in the 2" × 2" aperture. Figure 17 shows the plot of RV versus phase for He II λ4686. The phase is

TABLE 1

RADIAL VELOCITIES OF STRONG LINES IN THE IDS SPECTRA OF R136a (nonrectified)
(km s^{-1})

JD (−2,445,000)	Phase	[O III] λ5007	He II λ4685.685
4" × 4" Aperture			
309.719	0.597	287	424
310.685	0.818	250	327
311.655	0.040	276	366
312.575	0.250	240	404
313.606	0.485	287	398
313.685	0.503	298	359
314.664	0.727	231	340
315.601	0.941	254	347
315.676	0.958	271	372
mean		266	371
σ		23	32
2" × 2" Aperture			
309.733	0.600	247	398
310.692	0.820	257	359
311.668	0.042	257	327
312.591	0.253	237	359
313.615	0.487	256	417
313.676	0.501	268	424
314.647	0.723	272	424
315.684	0.960	276	417
mean		259	391
σ		13	37

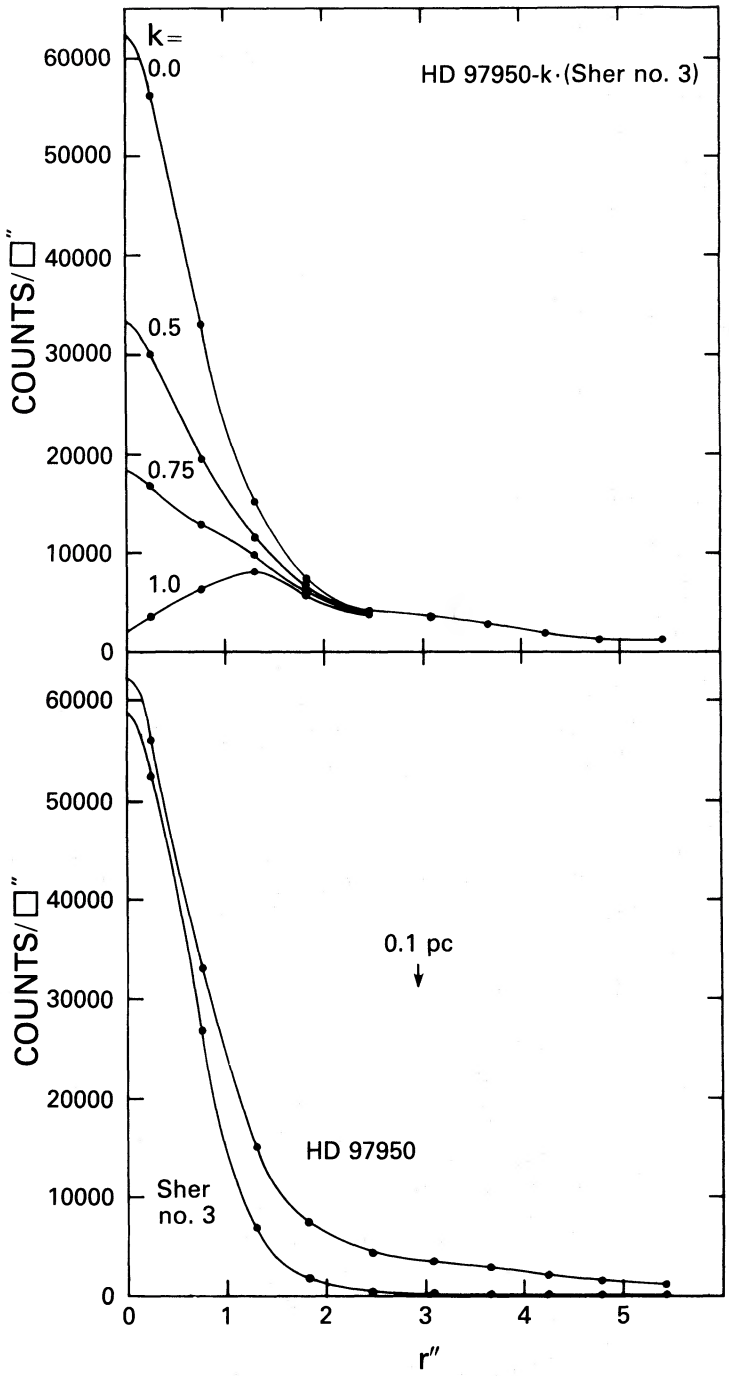

FIG. 15.—(*bottom*) Radial surface brightness (CCD counts arcsec^{-2}) vs. the radius from the center of HD 97950 and Sher No. 3 in the *W* filter (λ4700). The curve through the HD 97950 data is a hand-drawn fit, while that through the Sher No. 3 data is a fit to the seeing profile of Moffat (1969) with $R = 1\farcs33$ and $\beta = 3.2$. (*top*) Net surface brightness $I_{\rm HD\ 97950}(r) - kI_{\rm Sher\ No.\ 3}(r)$ for different values of the constant k.

based on the circular orbit of Moffat and Seggewiss (1983), with amplitude $K = 37$ km s^{-1} and period $P = 4\overset{\rm d}{.}377 \pm 0\overset{\rm d}{.}003$ (more likely than the alias $1\overset{\rm d}{.}2955$). We note that *the present orbit derived with the* 4″ × 4″ *aperture has an amplitude and phase compatible with the previous values.* The 2″ × 2″ aperture RV data appear to be too noisy to provide any useful information.

If due to a single W-R binary system, the RV amplitude is very low. This could be explained by a very low value of the orbital inclination ($i \approx 10°$), or unusually low mass of the companion. An alternate, less contrived explanation for the low amplitude is that of dilution of the orbital RV amplitude by line blending with other W-R stars of similar spectra, whose light falls in the aperture. This is a plausible explanation since we already have independent evidence for more than one W-R star in R136a.

If there are n W-R stars, each with similar He II λ4686 lines, but only one exhibits a RV orbit with amplitude K_1, then the

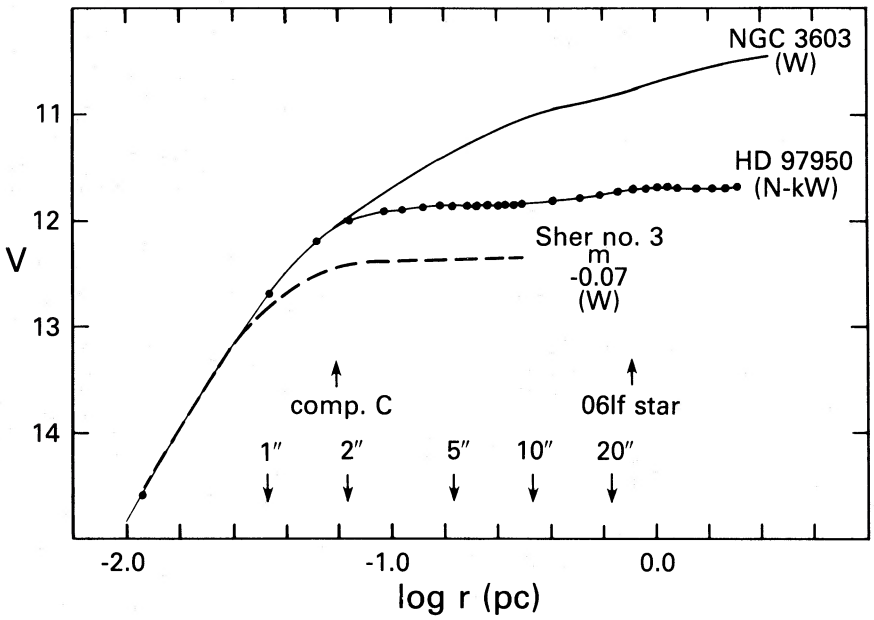

FIG. 16.—Accumulative radial surface brightness distribution in magnitudes, with the same zero point as in Fig. 14, of the net He II λ4686 emission centered on HD 97950AB. Since there are no other isolated W-R stars for comparison on the same image (although the O6 If star Sher No. 18 appears to cause a small increase at $r \approx 23''$ from the center), we show instead Sher No 3 and the overall cluster distribution in the W filter, force fitted asymptotically to the innermost part of HD 97950. $N - kW$ represents the subtraction of the N and the W images with the value of the constant k which nulls non–emission line stars.

observed amplitude will be $K_{obs} \approx K_1/n$. Table 2 lists pairs of possible values of n and the resulting mass function $f_1(m)$ for R136a (4″ × 4″). The same method has been applied to HD 97950 by Moffat and Niemela (1984). Compared to mass functions of other isolated WNL (+O) stars in the LMC (Moffat 1985): FD 24, 55, 62, 67 and 71, with $f(m) = 0.8$–$4.2\ M_\odot$, the *best* range of $f_1(m)$ here is for $n = 4$–5, with a possible range of $n = 3$–6. If the orbiting W-R star with $P = 4^d.377$ has weaker emission lines than the other W-R stars, $n \rightarrow 6$ is favored; if stronger, $n \rightarrow 3$. We note that it is quite reasonable to find at least one SB among a group of three to six W-R stars since the W-R + O binary frequency is estimated to be $\gtrsim \frac{1}{3}$ (cf. Moffat and Shara 1985).

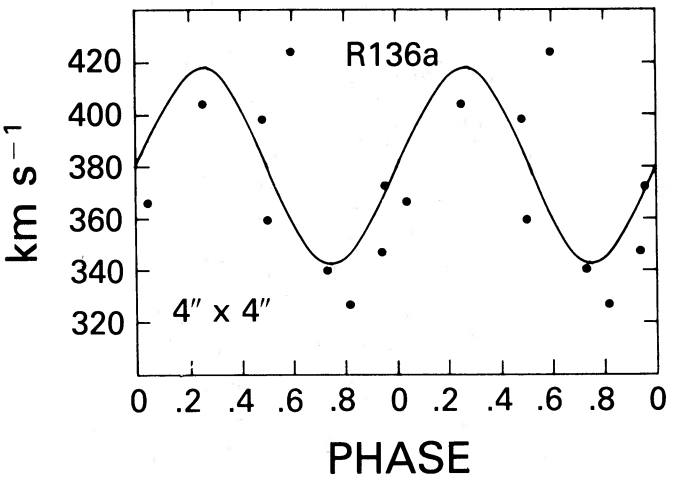

FIG. 17.—Radial velocity of He II λ4686 in the 4″ × 4″ aperture of R136a vs. phase, based on the ephemeris of Moffat and Seggewiss (1983): time of γ-passage (W-R star in front) JD 2,443,840.81 ± 0.13 + (4.377 ± 0.003) E. The curve represents the previous orbit ($K = 37$ km s^{-1}) shifted in RV to $\gamma = 380$ km s^{-1}.

Now we compare the total W-R population in R136 with that in the 30 Dor cluster (within a circle centered on R136):

$$\frac{N_{\text{W-R}}(\phi = 7'')}{N_{\text{W-R}}(\phi = 2'')} = \frac{4 \rightarrow 7}{16 + (4 \rightarrow 7)}.$$

The numerator is based on three to six W-R stars in R136a together with R136c, while the denominator equals the numerator plus the number of W-R stars based on the present data as well as those of Moffat *et al.* (1985). Note that R140 contains (at least) three W-R stars. This ratio reduces to the range $\frac{1}{5}$–$\frac{1}{3}$ with a most likely value $\frac{1}{4}$, quite similar to the visual light ratio of the same areas:

$$\frac{L_{\text{vis}}(\phi = 7'')}{L_{\text{vis}}(\phi = 2')} = \frac{1}{4},$$

TABLE 2

CORRECTED MASS FUNCTION FOR R136a (4″ × 4″)

n	$f_1(m)/M_\odot$	
1	0.02	
2	0.2	
3	0.6	[b]
4	1.5	[a] [b]
5	2.9	[a] [b]
6	5.0	[b]

NOTE.—This assumes that the true RV amplitude of the orbiting W-R component is $K_1 = nK_{obs}$, where $K_{obs} = 37$ km s^{-1}. The orbit is based on $e = 0$, $P = 4^d.377$ (Moffat and Seggewiss 1983).

[a] Best range.

[b] Possible range.

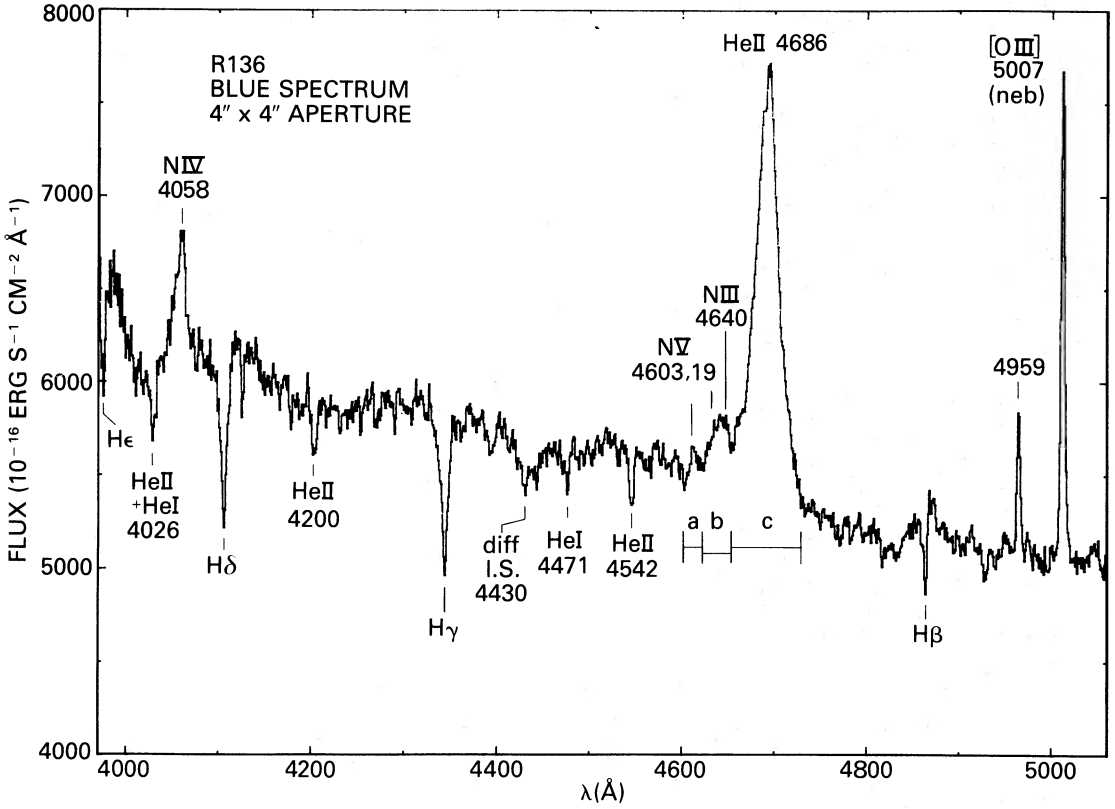

FIG. 18*a*

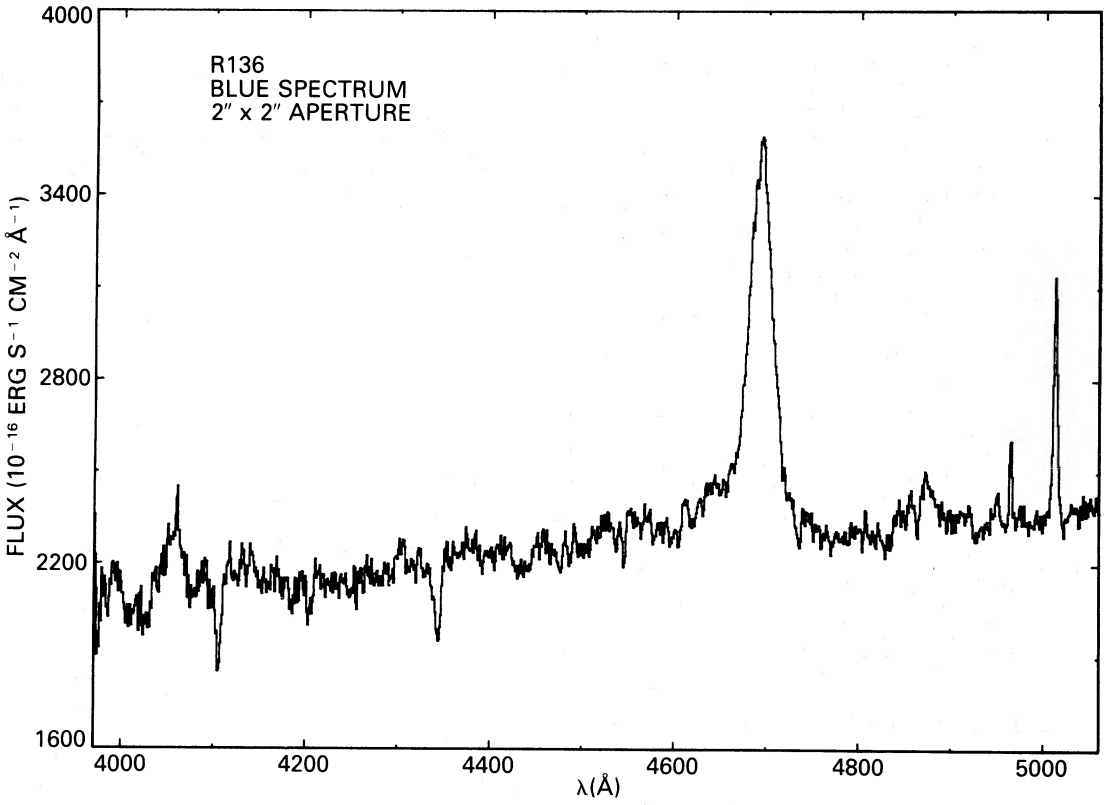

FIG. 18*b*

FIG. 18.—Flux-calibrated mean spectra of R136a (*a*) in the blue through a 4″ × 4″ aperture, mean of eight individual spectra; (*b*) in the blue through a 2″ × 2″ aperture, mean of six spectra; and (*c*) in the red through a 4″ × 4″ aperture, mean of two spectra. Salient features are identified on the 4″ × 4″ spectra. The redward sloping continuum for the 2″ × 2″ aperture is due to the effects of differential refraction (see text).

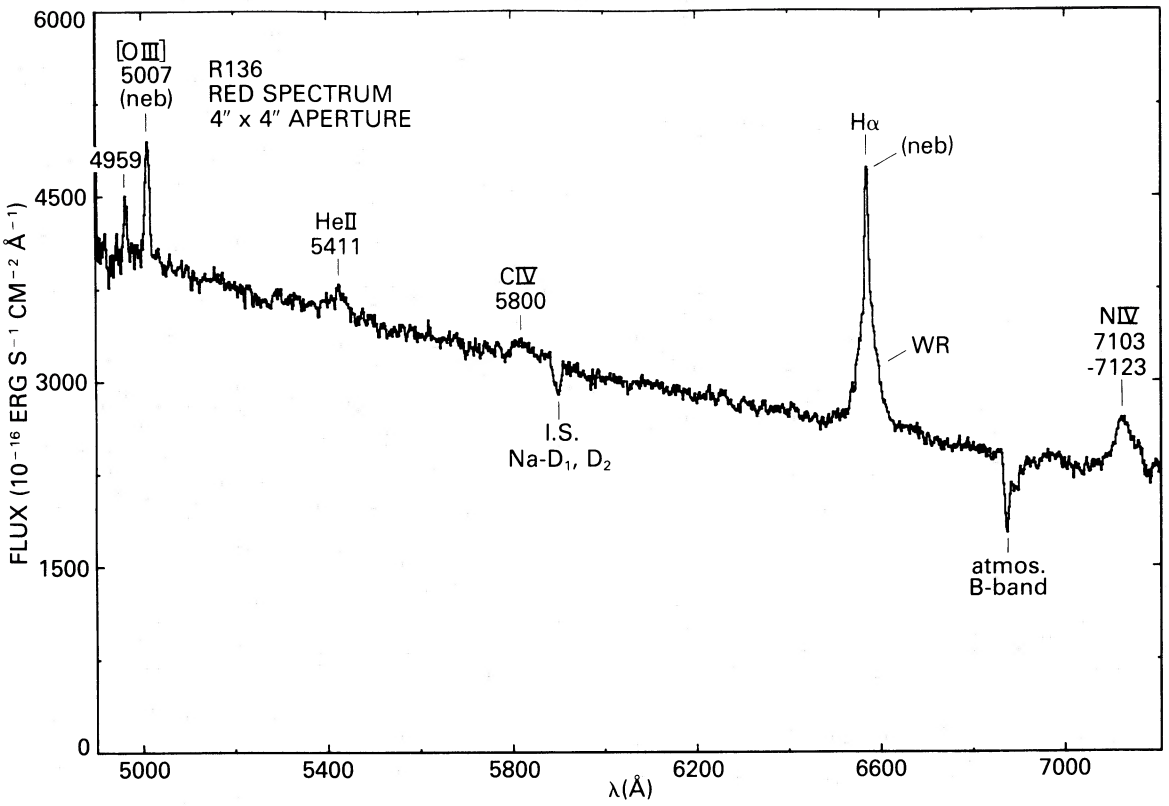

FIG. 18*c*

on the basis of the radial light distribution in Figure 7. This implies that the relative W-R population is similar within R136 to that of its surroundings.

By co-adding all 2″ × 2″ and all 4″ × 4″ spectra centered on R136a, we can increase the signal-to-noise ratio. This co-addition is justified by the fact that there are no significant profile variations and only low-amplitude ($\lesssim 1$ Å) RV variability. Figure 18 shows the flux-calibrated mean spectra.[8]

From Figure 18*a*, we derive equivalent widths (cf. Table 3) of the main features in the 4″ × 4″ spectrum of R136a:

i) *Emission*

After subtracting the N V λ4619 line off the blended N III λ4640 + N V λ4619 feature (*b* in Fig. 18*a*) and assuming equal strengths for N V λ4603 and N V λ4619 (a reasonable assumption based on inspection of narrow-line WN stars of different ionization class), we obtain the following equivalent widths:

N III λ4640/N IV λ4058/N V λ4603

$$= -1.18 \text{ Å}/-1.41 \text{ Å}/-0.24 \text{ Å} .$$

The N III/N IV ratio suggests a subclass WN5/6, while N IV/N V yields WN6, using the quantitative work of Conti, Leep, and Perry (1983) as a guide. We adopt WN6 as the best overall approximation for the dominant W-R spectrum in the central 4″ × 4″ of R136a. We note that the N lines appear weak compared to He II λ4686. This is typical for WN stars in the LMC, where He II lines are about twice as strong as in their galactic counterparts (Smith and Willis 1983).

ii) *Absorption*

Melnick (1983; private communication) has shown from direct observations near R136 that He I λ4471 is *not* noticeably contaminated by nebular emission of the same line in R136. We can also estimate the degree of contamination on the basis of nearby observations of the 30 Dor Nebula by Peimbert and Torres-Peimbert (1974), assuming constant nebular line ratios across the nebula. We estimate a ~15% contamination of our observed equivalent width of He I λ4471 in Table 3. Allowing for this, we can use the corrected ratio of equivalent widths,

$$\frac{\text{He I } \lambda 4471}{\text{He II } \lambda 4542} = 0.5 ,$$

to obtain a dominant absorption spectrum of O5 (or possibly O6). The 2″ × 2″ aperture spectrum (Fig. 18*b*) is noisier but tends to show a slightly cooler O type.

The overall 4″ × 4″ spectrum of R136a appears to be close to

$$\text{WN6} + \text{O5} ;$$

the derived type may very well be a function of seeing, detector, and aperture size and orientation. For comparison, most recent determinations of the spectral type are by Ebbets and Conti (1982), who found WN4.5 + abs in a 3″ × 1″ (east-west × north-south) aperture; Melnick (1983): WN4.5 + O6–7 in 3″ × 0.″5 (east-west × north-south), compared to his co-added flux spectra of a complete sample of *surrounding* stars,

[8] Note that the 2″ × 2″ aperture spectrum discussed below slopes up to the red, while that for 4″ × 4″ slopes up to the blue, the latter being expected for hot, mildly reddened stars, as is the case here. This difference is due to the effects of differential refraction in the 2″ × 2″ aperture, which amounts to 0.″7 per 1000 Å at airmass 1.3 and mean wavelength ~4500 Å (Allen 1973), typical for these spectra. On the other hand, differential refraction has negligible effect on the *spectral features*, which are always narrower than 100 Å. Over this range in wavelength, differential refraction is only ~0.″07, i.e., much smaller than the aperture used.

TABLE 3

EQUIVALENT WIDTHS FROM THE 4″ × 4″ MEAN SPECTRUM
(Å)
A. Absorption

STAR	N IV λ4058	N V λ4603	N III λ4640 +N V λ4619	He II λ4686	[O III] λ4959	[O III] λ5007
R136a	−1.41	−0.24	−1.42	−13.41	−0.67	−2.53
HD 97950 ...	−2.11	−1.01	−7.56	−24.36	...	...

B. Emission

STAR	He II + He I λ4026	λ4101 Hδ	λ4200 He II	λ4340 Hγ	λ4471 He I	λ4542 He II
R136a	0.28	1.18	0.27	1.29	0.13	0.27
HD 97950 ...	0.24:	0.50:	...	0.52:	0.08:	0.18:

NOTE.—N V λ4603, N III λ4640 + N V λ4619, and He II λ4686 were obtained as shown in Fig. 18*a*. For narrow lines like [O III], the estimated standard errors in W_e are ∼0.1 Å. This accounts for the deviation of the observed flux ratio (3.8) of λ5007/λ4959 from the standard value 2.9.

WN6 + O5–6 (like our present estimate for R136a); and Moffat and Seggewiss (1983): WN6 + O3–4 in 6″ × 2.″5 (east-west × north-south). We also do not exclude the possibility that different investigators might interpret the same spectrum in different ways. Nevertheless, the difference between O3–4 and O6–7 is probably significant and is likely a result of the multiple component nature of R136.

The UV spectrum exhibits an intermediate WN plus very early O type (Savage *et al.* 1983) and may differ from the visual spectrum due to different weighting factors of stars of various temperature in the UV versus the visible part of the spectrum. Thus, one might expect O3 stars to dominate more in the UV than in the visible, as seems to be the case.

In Figure 19 we compare the fluxed spectrum of R136a over a range of 340 Å centered at $\lambda \approx 4600$ Å with spectra obtained during the same observing run of five other W-R stars of similar type (WN6) located within the 30 Dor complex. While R134, R136c, and R145 show relatively narrow emission lines, R140b and especially the binary R130 reveal much broader lines. R136a lies somewhere in between, as might be expected if it consists of several narrow-line WN components. In Table 4, we compare flux (i.e., not equivalent width) ratios of He II λ4686 emission and nearby continuum between R136a and three WN6 stars. This is done in matched aperture pairs. From this we see that the 2″ × 2″ center of R136a could contain ∼3 W-R stars with average emission strength like R140b (R134 and R145, being brighter than R140b in the continuum, appear to possess greater line strengths as well). This number is compatible with the number of W-R stars deduced to lie in R136a on the basis of the CCD images and the low RV orbit. Furthermore, R136a emits as much continuum light at λ4700 as six stars like R134 ($V = 12.4$) in 2″ × 2″ or about eight stars like R145 ($V = 12.0$) in 4″ × 4″. Allowing for differences in seeing, this is in line with the integrated magnitudes in Figure 7. In summary, it appears that the equivalent widths of the W-R emission lines in R136a are diluted by a factor of ∼3–5 by non–W-R (i.e., mainly O star) light.

TABLE 4

FLUX RATIOS OF R136a AND THREE RESOLVED W-R STARS OF SIMILAR WN SUBCLASS

STAR RATIO	APERTURE SIZE	FLUX RATIO: He II λ4686 Emission	FLUX RATIO: Continuum at λ4700
R136a/R134	2″ × 2″	1.5	6
R136a/R140b	2″ × 2″	3	8.5
R136a/R145	4″ × 4″	1.7	8

From the net He II λ4686 CCD images we saw that W-R emission arises in an extended area in R136a. This can be compared to spatially resolved spectroscopy. Figure 20 displays the rectified 2″ × 2″ spectra around He II 4686 taken at nine adjacent positions in a 6″ × 6″ region centered on R136a. We note first that the continuum flux level at $\lambda \approx 5000$ Å diminishes away from the center, as expected on the basis of the CCD observations:

$$\frac{f(r \leq 3.''4)}{f(r \leq 1.''1)} = \frac{9000}{2200} = 4.1(1.5 \text{ mag}) .$$

The numerator corresponds to a 6″ × 6″ square, the denominator to a 2″ × 2″ square. Thus, with $V(r \leq 3.''5) = 10.0$ mag from photoelectric diaphragm photometry (cf. Moffat and Seggewiss 1983), this leads to $V(r \leq 1.''1) \approx 11.5$ mag, somewhat fainter than the 11.0 mag derived from the CCD results in Figure 7. The difference is likely due to differences in seeing and due to the inclusion of the He II λ4686 emission line in the broad CCD filter, which tends to peak in strength toward the center of R136a. Note that no background core light has been allowed for in either case.

Even though there may be some overlap between *adjacent* spectra in Figure 20, the differences in emission-line strength and profile are often extreme, as noted on the basis of long-slit spectroscopy by Moffat and Seggewiss (1983) and Melnick (1983). This implies that different W-R stars fall in different apertures according to their positions in R136a. The strongest line emission is seen in the central and western apertures, where components A and B dominate to produce a ∼WN6 spectrum. In the eastern central aperture, we see narrow emission (component D?) corresponding more to WN7. Again, we see evidence for the presence of at least three distinct W-R stars within R136a. We note also a variation (though more subtle) in O-type spectrum going from the 2″ × 2″ to the 4″ × 4″ aperture centered on R136a (see above).

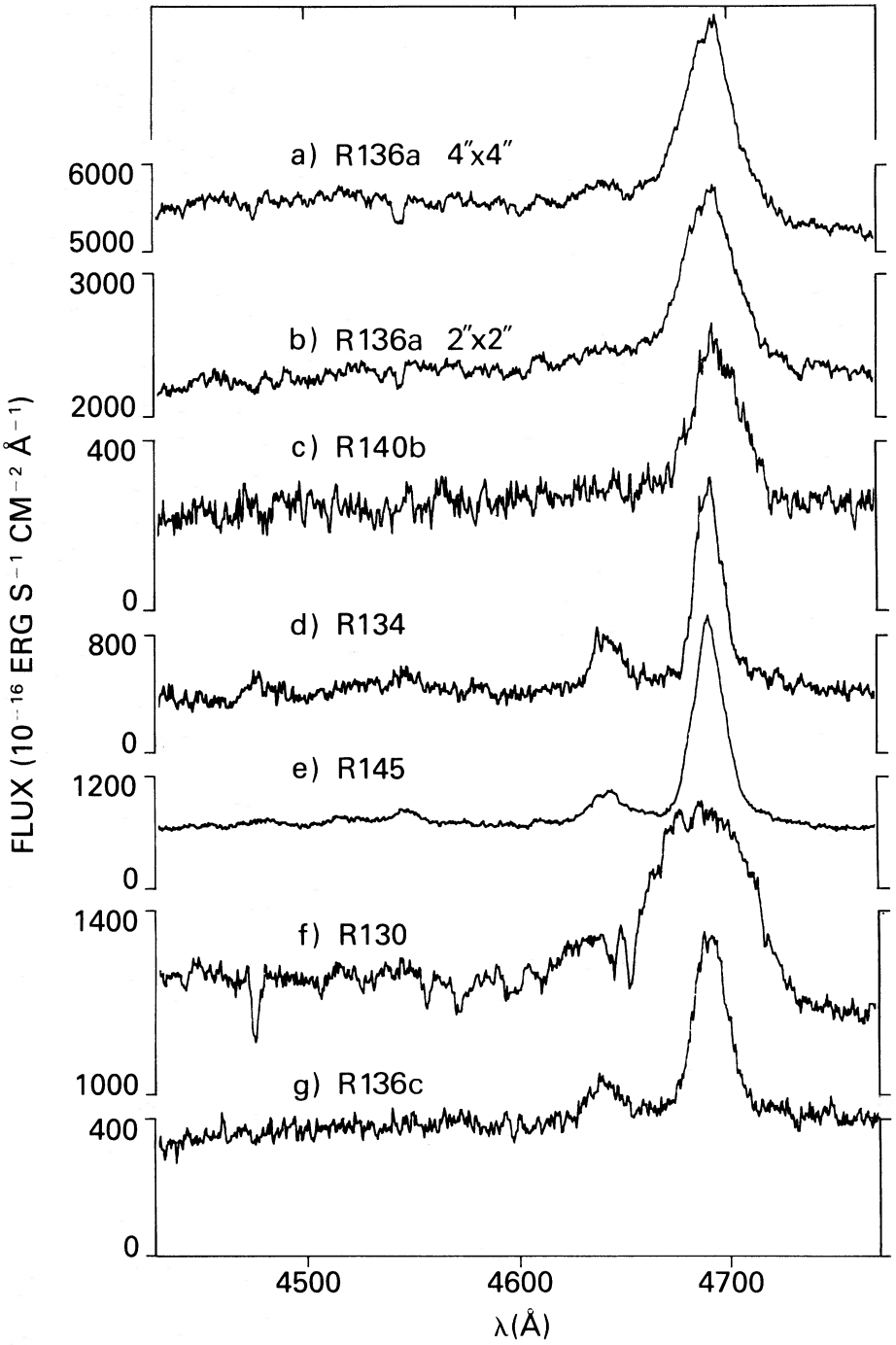

FIG. 19.—IDS flux spectra from the same run, in a region 340 Å wide centered at 4600 Å, of (*a*) R136a in 4″ × 4″, (*b*) R136a in 2″ × 2″, (*c*) R140b (WN6:) in 2″ × 2″, (*d*) R134 (WN6) in 2″ × 2″, (*e*) R145 (WN6) in 4″ × 4″, (*f*) R130 (WN6 + BIIa) in 4″ × 4″, and (*g*) R136c (WN6:) in 2″ × 2″. Note the revised WN subclass for R130 compared to Breysacher (1981), who gave WN3:. The dominent strength of N III λ4640 is evident in (*f*).

How much light from R136a is in the form of nebular emission? We attempt to answer this on the basis of (1) Figure 21, which shows a 2″ × 2″ aperture spectrum for R136a compared to a 2″ × 2″ spectrum of the nebula—reduced identically as R136a—25″ west of R136a (the "sky" positions for each appeared to have about equally low nebular emission), and (2) Figure 22, which depicts the absolute nebular strength from the same nebular area as in Figure 21, but using a more distant, dark part of the sky as a reference. All these spectra were obtained during the same night and are shown in the same scale in Figures 21 and 22. From these figures, we conclude that continuous nebular light contributes negligibly to the spectrum of R136a, while only the nebular lines, e.g. [O III] λ5007, which has similar strength in Figures 21*a*, 21*b*, and 22, make some small contribution when considering broadband photometry. From the strength of the [O III] lines (short-

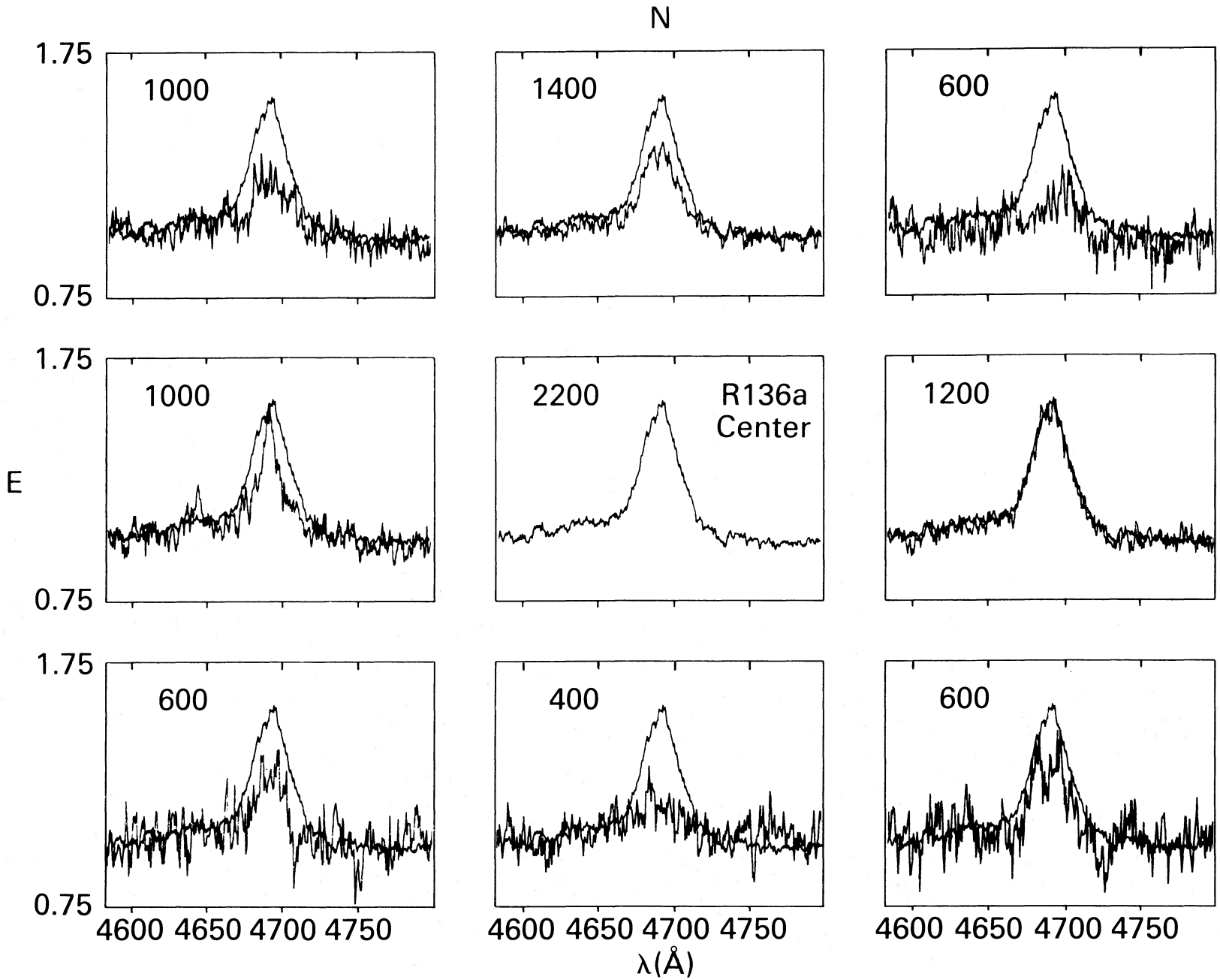

FIG. 20.—Rectified IDS spectra in a ~220 Å region centered near He II λ4686 across the face of R136a. Each spectrum refers to a 2″ × 2″ region on the sky in adjacent areas that are arranged in the same way as the spectra are here. The mean central spectrum is superposed on each of the others for comparison. The continuum flux in units of 10^{-16} ergs s^{-1} cm^{-2} $Å^{-1}$ at $\lambda \approx 5000$ Å is given for each spectrum; it is 400 units for R136c just off the lower left.

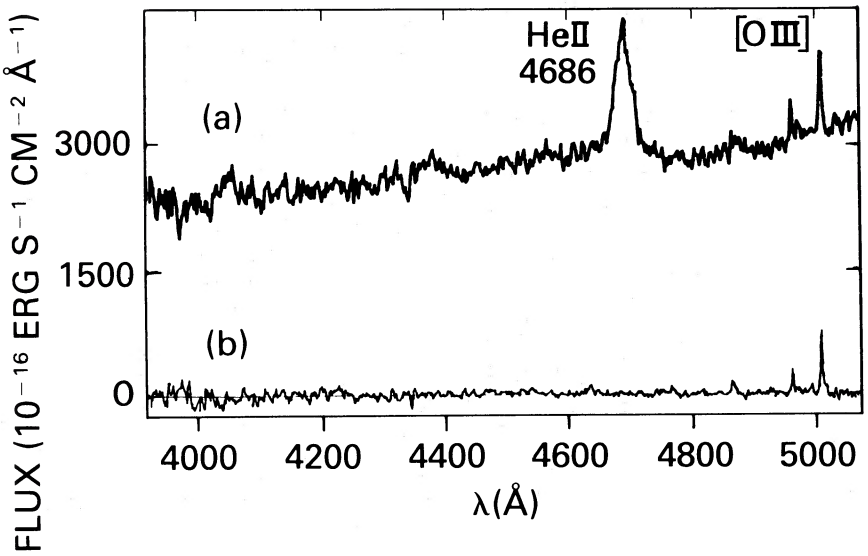

FIG. 21.—IDS fluxed spectra in the blue in a 2″ × 2″ aperture centered (*a*) on R136a and (*b*) on a nebular region 25″ west of R136a. Both spectra were obtained in the same way ("sky" channel 60″ to the east and the west respectively) during the same night. Flux units as in Fig. 20.

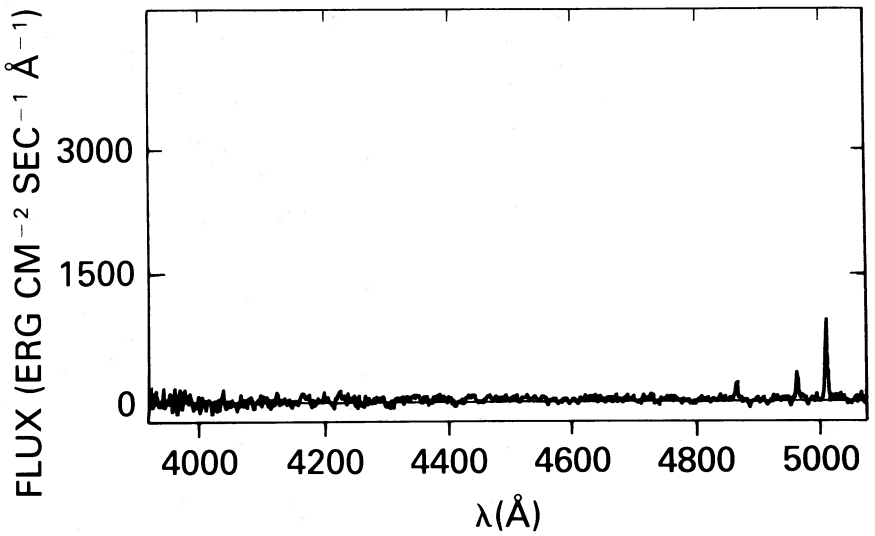

FIG. 22.—IDS fluxed spectrum as in Fig. 21 of the same nebular region 25″ west of R136a but with dark sky background well removed from the 30 Dor nebula

wavelength end of the broad-band *V* filter) and the Hα line (long-wavelength end in *V*) and an upper limit on the nebular continuum, we estimate

$$\frac{f_{\rm neb}}{f_{\rm R136a}} < 2\% ,$$

i.e., $V_{\rm neb} > 16$ in 2″ × 2″ centered on R136a. Thus, by far most of the visual light from R136a must be stellar in origin.

b) The core of NGC 3603

As in the core of R136, intercomparison of the seven individual IDS spectra of HD 97950 (4″ × 4″ available only) shows no significant line-profile variations with time. Also as for R136a, HD 97950 exhibits radial velocity variations, on the basis of the two strongest W-R lines He II λ4686 and N IV λ4058 (cf. Table 5). The latter line is weaker and yields less precise RVs.

TABLE 5

RADIAL VELOCITIES OF STRONG LINES IN THE IDS SPECTRA OF HD 97950 (nonrectified, 4″ × 4″ aperture) (km s^{-1})

JD (−2,445,000)	Phase[a]	N IV λ4057.759	He II λ4685.685
309.847	0.753	−123	+78
310.855	0.020	+107	+110
311.843	0.282	+33	+148
312.841	0.547	+3	+72
313.817	0.806	−137	+8
314.860	0.082	−86	+142
315.822	0.337	−19	+148
mean		−32	+101
σ		89	52

[a] Based on ephemeris JD 2,444,258.39 ± 0.10 + 3.7720 ± .0003 E, from Moffat and Niemela 1984.

Although the He II λ4686 emission line is somewhat stronger in HD 97950 than in R136a, the RV dispersion about the mean is larger in HD 97950, suggesting a larger amplitude RV orbit. The RV-phase plot in Figure 23 reveals good agreement with a previously determined orbit based on independent data (Moffat and Niemela 1984). The RV amplitude is close to $K \approx 60$ km s^{-1} for all sets of data.

As noted before for HD 97950 by Moffat and Niemela (1984), the low RV amplitude can be most readily explained by dilution effects, with a total of $n \approx 3$ W-R stars assumed to be of similar line strength and subclass in the spectrum of HD 97950. These three W-R components are likely related to the visual components A, B, and C, as noted above with reference to the net emission CCD images.

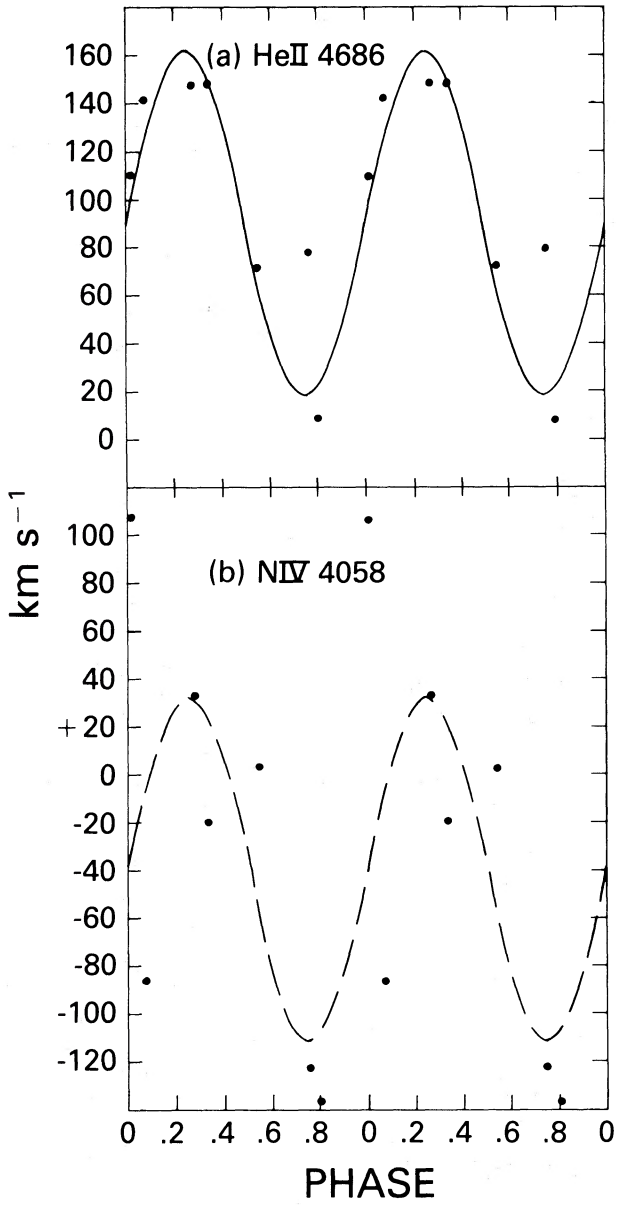

FIG. 23.—Radial velocity of the emission lines (*a*) He II λ6486, (*b*) N IV λ4058 in the 4″ × 4″ aperture, vs. phase, based on the ephemeris of Moffat and Niemela (1984) for HD 97950—cf. Table 5. The curve represents the previous orbit ($K = 72$ km s^{-1}) shifted in RV to $\gamma = +90$ km s^{-1} for He II and $\gamma = -40$ km s^{-1} for N IV.

Now we compare the total W-R population in HD 97950 with that in NGC 3603 as a whole:

$$\frac{N_{\text{W-R}}(\text{HD 97950}, \phi = 5'')}{N_{\text{W-R}}(\text{NGC 3603}, \phi = 1')} = \frac{3}{3},$$

i.e., there are no W-R stars in NGC 3603 outside the core, neglecting the Of star Sher No. 18, although it may be on its way to the WN stage. The visual light ratio in the same respective regions (cf. Fig. 14) is:

$$\frac{L_{\text{vis}}(\text{HD 97950}, \phi = 5'')}{L_{\text{vis}}(\text{NGC 3603}, \phi = 1')} = \frac{1}{3}.$$

Thus, in contrast to 30 Dor, all the W-R stars of NGC 3603 are located in the core region. This statement applies within the obvious limitations of small number statistics.

We now turn to the mean spectrum of HD 97950 (4″ × 4″ only) in Figure 24. Note that the spectrum slopes up toward the red due to the relatively large interstellar extinction ($A_v = 4.4$ mag) compared to R136 ($A_v = 1.2$ mag). From Figure 24 we determine equivalent widths (cf. Table 3) of the main features in the spectrum of HD 97950. In the same manner as for R136a, these lead to:

N III λ4640/N IV λ4058/N V λ4603

$$= -6.55 \text{ Å}/-2.11 \text{ Å}/-1.01 \text{ Å}.$$

The N III/N IV ratio implies a subclass WN6/7, while N IV/N V yields WN4/5 or WN8/9 following Conti, Leep, and Perry (1983). The best overall subclass is probably WN6, but the spectrum may include a mixture of subtypes.

With the absorption-line ratio He I λ4471/He II λ4542 = 0.5, the absorption spectrum corresponds to type O5. Thus, the best overall type for HD 97950 in the central 4″ × 4″ is WN6 + O5, like that for R136a. Conti, Leep, and Perry (1983) give WN7 + abs in a diaphragm of 3″ × 1″ (east-west × north-south) for HD 97950.

Finally, we compare the spectrum of HD 97950 across its face. In Figure 25 we show the 2″ × 2″ aperture, rectified spectra of the components A, B, C, and D in a restricted wavelength region near He II λ4686. Superposed on each is the 4″ × 4″ mean spectrum centered on AB. From Figure 25 we note that the emission-line spectrum is broadest and strongest in component B; C appears narrower within the limits of the higher noise level; while A is about the same as the mean AB spectrum, i.e., the W-R spectrum differs slightly from one component to another among A, B, and C. Star D is clearly non–W-R. It appears to be a visual double (Chu, private communication) and was classified O5 V by Moffat (1983*a*), like the absorption component of HD 97950, as well as other O stars in the immediate surroundings. This supports the evidence that most of the light from HD 97950 refers to a tight collection of W-R and O stars. On the basis of Walborn's (1973) series of short photographic exposures, none of components A, B, or C appears truly circular either; each is likely a multiple system. Also, nebular light is negligible in these spectra.

In summary, the spectra presented here show no evidence for abnormally bright stars with $M_v \lesssim -7$.

V. CONCLUSIONS

In their central 4″ × 4″, R136a and HD 97950 reveal similar optical spectra: WN6 + O5. In the UV, R136a appears to be

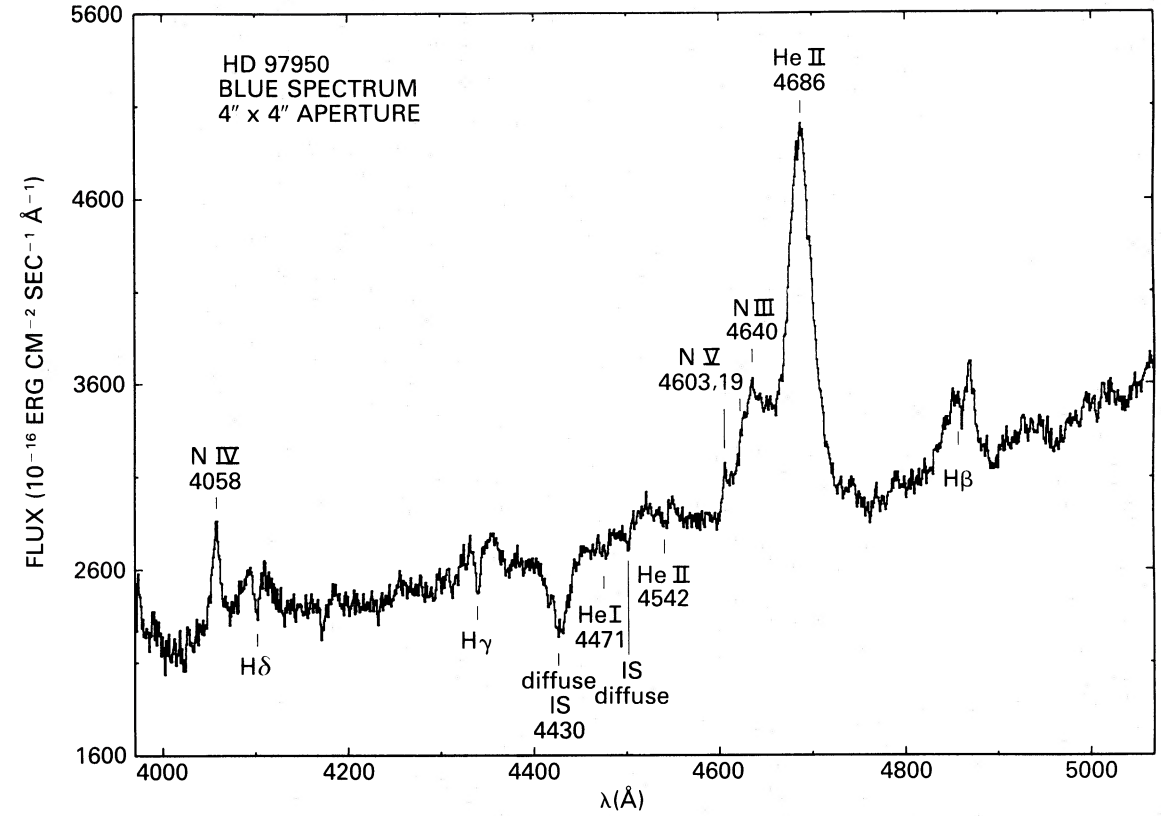

FIG. 24*a*

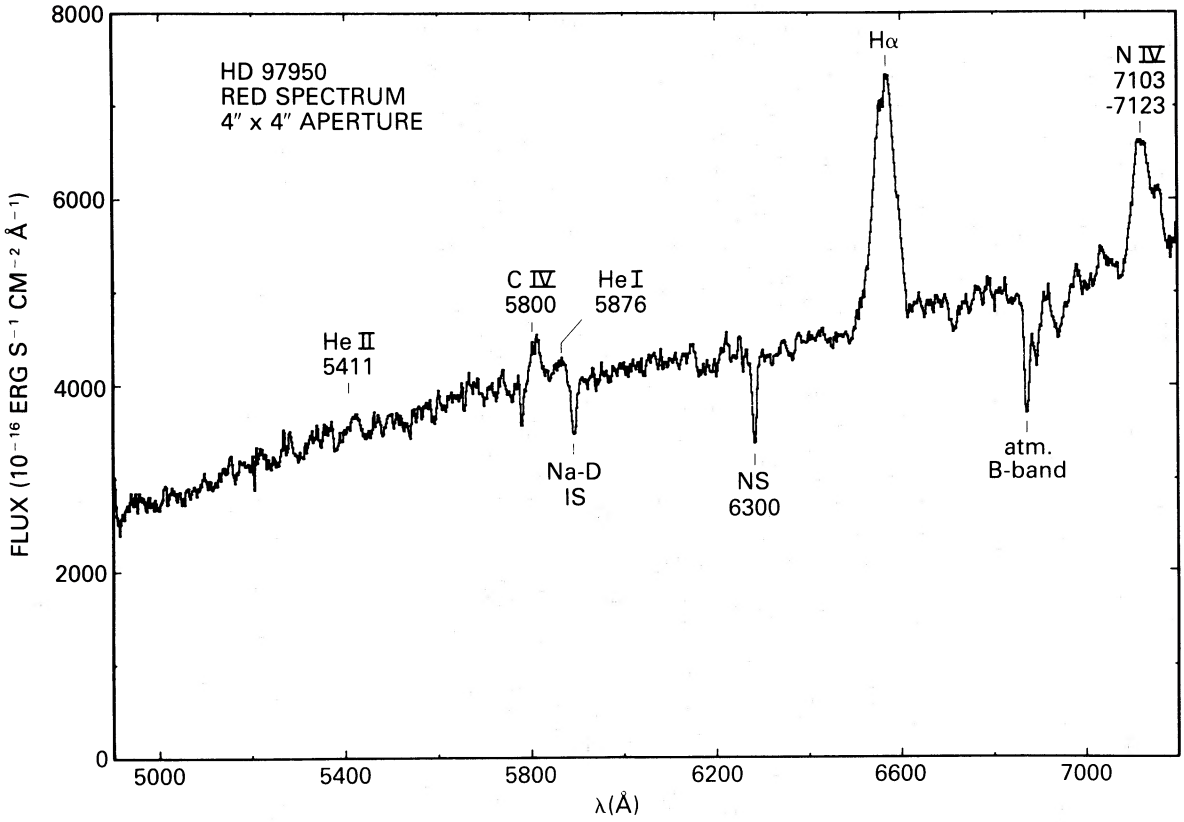

FIG. 24*b*

FIG. 24.—Flux calibrated spectra of HD 97950 in the 4″ × 4″ aperture for (*a*) the mean of six spectra in the blue and (*b*) one red spectrum. Salient features are identified.

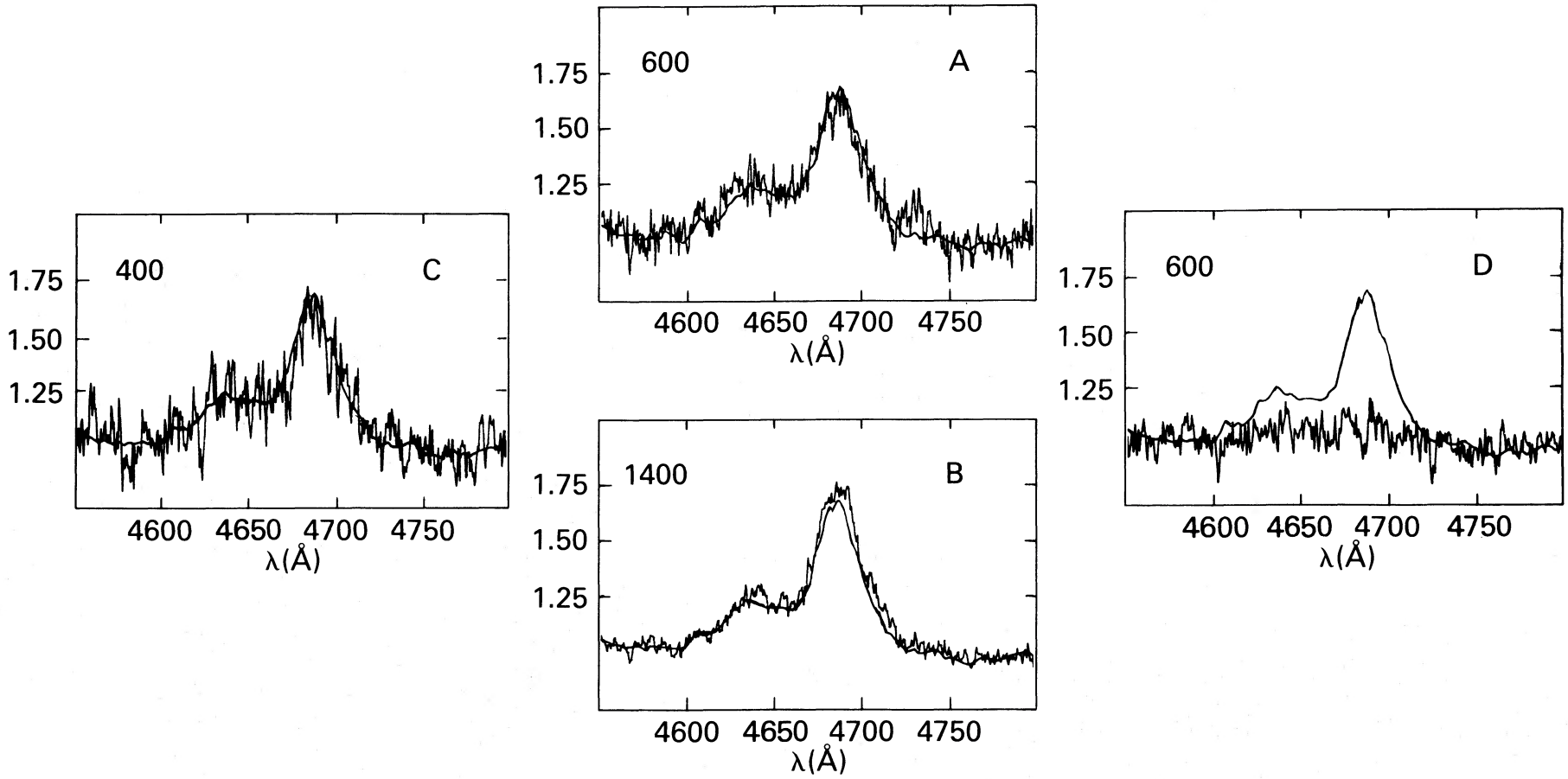

FIG. 25.—Rectified IDS spectra in a 250 Å region centered at λ4675 for the components A, B, C, and D of HD 97950. Each spectrum refers to a 2″ × 2″ region. The mean rectified spectrum of A and B combined in 4″ × 4″ is superposed on each for comparison. The continuum flux in units of 10^{-16} ergs s^{-1} cm^{-2} $Å^{-1}$ at $\lambda \approx 5000$ Å is indicated for each spectrum; it serves only as a rough guide where crowding is greatest and positioning the image is difficult.

dominated, not surprisingly, by hotter O3–4 stars while WN6 (like R144 or R145) prevails for the W-R component (Savage *et al.* 1983). Each object contains stars (whose spectra completly dominate the nebular emission) of normal magnitude (and hence also normal mass) up to $M_v \geq -8.4$ (≥ -8.0 if $V_0 - M_v = 18.2$ instead of 18.6) in R136a (only ≤ 0.4 mag brighter than the single nearby WN6 star R144) and $M_v \geq -8.0$ in HD 97950AB. These limits apply after subtracting off the background stellar light and could easily be reduced to $M_v \gtrsim -7.5$ (for each of components A and B, if assumed to be of approximately equal magnitude; each of these may in turn be multiple) for truly *individual* stars. High spatial resolution imagery will be needed to settle this definitively. The limits are based mainly on the broad-band CCD images, guided by the presence of the astrometric multiple components.

Each of R136a and HD 97950 contains *several* W-R stars, all of WN type and probably in the range of subclass WN5–7. The best estimate is that R136a contains four or five, and HD 97950 contains two or three, W-R stars of conventional brightness. This is based on: (*a*) the extended nature of the net He II emission, (*b*) the total amount of net He II emission compared to nearby average W-R stars, (*c*) change of spectrum across the object, and (*d*) the factor necessary to account for the dilution of the RV orbit in order to yield a normal mass function.

Since the present CCD/narrow-band survey for W-R stars appears to be complete within the central region of 30 Dor and NGC 3603, we can estimate the ratio of the number of W-R to O stars (of type O3–9):

i) in $\phi = 2'$ (the bulk of the 30 Dor cluster) around R136:

$$N_{W\text{-}R}/N_O \approx 200/300 = 0.07 ,$$

based on an extrapolation to type O9 of the initial mass function (IMF), $N(M)dM \approx M^{-\alpha}dM$, with slope $\alpha = 2.5$, of the ~ 60 observed stars of type earlier than $\sim$O5 (Melnick 1983);

ii) in $\phi = 1'$ (the bulk of the NGC 3603 cluster) around HD 97950:

$$N_{W\text{-}R}/N_O \approx \tfrac{3}{85} = 0.04 ,$$

based on a similar extrapolation of the ~ 17 stars of type earlier than $\sim$O5 (Moffat 1983*a*).

Within the uncertainties, both ratios are similar to each other and to the general ratio for the Galaxy, whether a burst of star formation occurred (e.g., in the form of a young cluster) or not (e.g., stars in the general field): cf. Moffat (1983*b*). Furthermore, the ratio of the *number* of O stars in 30 Dor to that in NGC 3603 is ~ 3.5, which is very similar to the ratio of the total light (~ 3) implied by Figures 7 and 14.

The (integrated) surface light distribution of both clusters appears to satisfy a King profile, from the smallest range (arc seconds) to the largest (arc minutes). From the overall distribution of W-R stars in 30 Dor (Moffat *et al.* 1985), the same profile extends out to $r \approx 100$ pc ($\sim 7'$). Not only is the outer linear dimension of the 30 Dor cluster larger by a factor of ~ 10 than that of NGC 3603, but their formal core radii also differ by a similar factor (0.21 pc versus 0.024 pc). These core radii are not much larger than the Gaussian core seeing radii; hence, they may only represent upper limits to the true core radii (r_c), if such are indeed applicable here. The important point to note is the general similarity of the light distribution of these two objects compared to globular clusters. Indeed, some globular clusters may have unresolved cores (cf. Mihalas and Binney 1981). Note that within $r = 0.5$ pc fixed radius (2.″0 in R136a, 15″ in NGC 3603), HD 97950 is intrinsically brighter than R136a.

Another important comparison concerns the relative gas content. From Table 6 we see that the observed mass of ionized hydrogen is ~ 50 times higher in 30 Dor than in NGC 3603. This is in stark contrast with the total stellar luminosity, which

TABLE 6

MASSES, RELAXATION TIMES, COLLAPSE TIMES, AND STELLAR DENSITIES FOR THE CORE REGIONS OF 30 Dor AND NGC 3603

A.

Object	r(H II)[a] (pc)	M(H II)[a] ($M_\odot$)	r_{lim}[b] (pc)	$M_v(r_{lim})$	r_i[c] (pc)	$M_v(r_i)$	$M_v(r_i) - M_v(r_{lim})$
30 Dor	~ 30	5×10^5	~ 15	-11.1	0.38	-9.2	1.9
NGC 3603	~ 7.5	1.0×10^4	~ 1.5	-9.9	0.051	-8.2	1.7

B.

Object		$M_*(r_{lim})$ ($M_\odot$)	$M_*(r_i)$ ($M_\odot$)	$N(r_i)$[d]	t_{rh}[e] (10^6 yr)	t_c[f] (10^6 yr)	$\frac{M_*(r_i)}{4/3\pi r_i^3}$ ($10^5\ M_\odot\ pc^{-3}$)
30 Dor	(i)	10^6	1.7×10^5	6×10^5	55	820	7
	(ii)	10^5	1.7×10^4	6×10^4	22	330	0.7
	(iii)	10^4	1.7×10^3	6×10^3	9	130	0.07
NGC 3603	(i)	3×10^5	6×10^4	2×10^5	1.7	26	1000
	(ii)	3×10^4	6×10^3	2×10^4	0.7	11	100
	(iii)	3×10^3	6×10^2	2×10^3	0.3	4	10

[a] From Goss and Radhakrishnan 1969; Mills, Turtle, and Watkinson 1978 give M(H II) $= 6 \times 10^5\ M_\odot$ for 30 Dor. Values are converted to a distance of 7.0 kpc for NGC 3603.

[b] Optical limiting radius (cf. Figs. 7 and 14) measured to similar slope of King profile.

[c] Internal radius corresponding to $r_i = 1.''5$ (~ 2 seeing radii).

[d] Total number of stars $M_*(r_i)/m$, where m = mean stellar mass $= 0.3\ M_\odot$.

[e] Reference relaxation time within r_i.

[f] Collapse time $\sim 15 t_{rh}$.

is only a factor of ~ 3 greater in 30 Dor than in NGC 3603. Assuming (1) the total stellar mass to be proportional to the total stellar luminosity (similar IMFs for both—a good assumption at least for massive stars—cf. Freedman 1984), and (2) most of the gas to be in ionized form, leads to a gas-to-star mass ratio which is $\sim 50/3 \approx 17$ times higher in 30 Dor than in NGC 3603. This is typical of the LMC to Galaxy ratio. Star formation appears to be active in the LMC, but less efficient than in the Galaxy. The reason for this may lie with the mean difference in gas density or in metallicity ($Z_{\rm LMC} = 0.008$, $Z_0 = 0.03$; cf. Peimbert and Torres-Peimbert 1974, 1976). Low gas density and low Z (less efficient cooling) lead to lower star-formation rates.

A question of great importance concerning the existence of a central supermassive object (noncollapsed or collapsed) is related to the core collapse time. If a putative supermassive star is not formed directly at the time of protostellar cloud collapse, one way to produce such might be through coalescence of stars in the final collapse stage of the core. Under certain assumptions (e.g., no hard binary formation) this could occur after about $15t_{rh}$, where t_{rh} is the reference relaxation time (Spitzer 1975):

$$t_{rh}(\mathrm{yr}) = 9.10^5 R_h(\mathrm{pc})^{3/2} N^{1/2} m(M_\odot)^{-1/2}/\log\,(0.4N)\,,$$

where R_h is the radius containing half the mass, N is the total number of stars, and m is the average stellar mass. Since the true core radius is not well established, we will take R_h to be about twice the seeing radius, i.e., 1".5. Converting to parsecs, we refer to it as r_i (internal radius) for R136a and HD 97950 in Table 6. Within this radius, the actual light/mass distribution is not well known; what *is* known is that the light that arises there is produced mainly by an unresolved group of stars with conventional masses ($\lesssim 100\ M_\odot$).

To obtain N, we first take a plausible range in total stellar mass for 30 Dor of 10^6, 10^5, and $10^4\ M_\odot$, The most likely value, $10^5\ M_\odot$, yields a ratio of total stellar-to-gas mass of 0.2, in the range of the typical conversion rates of gas into stars in H II regions, according to Lequeux *et al.* (1981). Also, one expects a total mass of $\sim 10^5\ M_\odot$ in the form of stars after integrating the IMF ($\alpha = 2.5$) to $M \geq 0.1\ M_\odot$, starting with ~ 60 stars earlier than $\sim$O5. We now assume that the mass scales with the visual luminosity (cf. Figs. 7 and 14); thus, e.g., NGC 3603 would have ~ 3 times less stellar mass than 30 Dor, whatever the value assumed for the mass of the latter. Finally, N can be obtained from the stellar mass in the given volume divided by the mean stellar mass m, taken to be $\sim 0.3\ M_\odot$. This the mean mass that results from integration of a power-law IMF with $\alpha = 2.5$; it enters only approximately linearly in the expression for t_{rh} ($N^{1/2}m^{-1/2} = M^{1/2}m^{-1}$, where M is the total mass).

For R136, we find a core collapse time of several times 10^8 yr, which is much greater than the nuclear burning age of $\sim 3 \times 10^6$ yr, based on the evolution of the most massive O stars. Hence, on the basis of the present work, it is unlikely that any supermassive star was formed, at least by coalescence. This is in stark contrast with Savage *et al.* (1983), who obtain a core collapse time of 900 yr, based on the assumption of a very small radius ($R_h \approx 0.002$ pc = 0".008) and on an unrealistic IMF with $N = 40$ and a large *mean* stellar mass $m = 50\ M_\odot$. Here we find that R136 is not even fully relaxed. We emphasize that the calculated outcome depends critically on the initial assumptions.

The central star density within $r = r_i$ in R136a is $\sim 10^5\ M_\odot$ pc^{-3}, which is just below the maximum density observed or deduced for galactic globular clusters: $\sim 3 \times 10^5\ M_\odot$ pc^{-3} (Peterson and King 1975). Note that for a normal IMF, stars of mass greater than $1\ M_\odot$ comprise barely half the total mass. Thus, after $\sim 10^{7-8}$ yr when all the O and B stars have evolved, the central cluster of 30 Dor can be expected to resemble some of the medium-age populous clusters known in the LMC.

For NGC 3603, the situation appears to be somewhat different. The core relaxation time is in the range of $\sim 10^6$ yr. Thus the core of NGC 3603 may be relaxed. This is compatible with the fact that, unlike the 30 Dor cluster, all the W-R stars in NGC 3603 are located in its core; i.e., the most massive stars (the assumed progenitors of the present W-R stars) have had time to diffuse by dynamical interaction and equipartition of kinetic energy to the core region. The unambiguous presence of at least one massive close binary in the core may be related to the fact that the core of NGC 3603 is well advanced in its dynamical evolution; the formation of tight binaries may prevent a final gravothermal collapse. Calculations of postcollapse evolution allowing for the formation of tight binaries yield singular mass distributions of the form $\rho \approx r^{-2}$ (Inagaki and Lynden-Bell 1983). This is observationally difficult to distinguish from a King profile with $r_c \to 0$, i.e., $\rho \to r^{-3}$. It is possible that, with core radius (0.024 pc) well below even the smallest in the range known for galactic globular clusters [$0.2 < r_c(\mathrm{pc}) < 16$; Peterson and King 1975], NGC 3603 may be indeed approaching this state.

The basic reason for the difference beteen the 30 Dor and NGC 3603 clusters must lie in their different degree of compactness. While NGC 3603 is ~ 10 times smaller than the 30 Dor cluster (core or halo), it still contains a relatively high mass, only ~ 3 times less than the 30 Dor cluster. Thus the stellar density is $\sim 10^3/3 \approx 300$ times higher in NGC 3603 (core or halo). This in turn may be related to the higher efficiency of star formation in the Galactic object, and to a higher degree of relaxation.

Finally, we note that there is now little evidence, if any, to support the hypothesis of a superluminous (= supermassive) star of the kind proposed by Savage *et al.* (1983) with mass $2100\ M_\odot$ and radius $50\ R_\odot$ (or even a group of stars dominated by a less massive but still supermassive star: Chu, Cassinelli, and Wolfire 1984) at the core of 30 Dor. This applies also to NGC 3603 and, by extrapolation, probably also to other similar but poorly resolved extragalactic giant and supergiant H II regions. Besides the evidence presented here against the existence of supermassive stars, we note two other arguments:

1. The gravitational redshift predicted for the supermassive star (Savage *et al.* 1983) in R136 is $GM/cR \approx 27$ km s^{-1}. While Ebbets and Conti (1982) derived an H absorption line *redshift* of $\sim$50–100 km s^{-1} on the basis of a single image tube spectrum, Moffat and Seggewiss (1983) found a *blueshift* of 26 ± 7 km s^{-1} based on H absorption line measurements on several dozen image tube spectra. Such a blueshift is typical of *normal*, hot stars with dense winds (Conti, Leep, and Lorre 1977). We consider it contrived to require both a gravitational redshift of ~ 27 km s^{-1} and a wind-type blueshift of ~ 53 km s^{-1}.

2. No significant photometric variability has been observed on time scales ranging from hours to years (cf. Moffat and Seggewiss 1983). A very massive object ($\sim 2000\ M_\odot$) is expected to pulsate with a period of the order of a day (Ledoux, Noels, and Boury 1982). Occasional, even large, fluctuations are not excluded by the available data, but they are not favored either.

We therefore support the hypothesis that the luminous fuzzy cores of giant and supergiant H II regions probably represent the dense cores of young, populous clusters like those seen at various ages in the LMC. Although NGC 3603 verges on being a populous cluster in the LMC sense, it is a rare type of object in the Galaxy and indeed may not survive in its present state for long.

A. F. J. M. is grateful to the Alexander von Humboldt Stiftung (F. R. Germany) and the Natural Sciences and Engineering Research Council of Canada for financial assistance. M. M. S. and A. F. J. M. thank Dr. P. Seitzer for instruction in use of the CTIO 4 m prime focus CCD camera. We thank Mr. M. Potter for his able and patient assistance in image processing. We appreciate the numerous valuable comments of the referee, Dr. Y.-H. Chu.

REFERENCES

Allen, C. W. 1973, *Astrophysical Quantities* (3rd ed.; London: Athlone), p. 124.
Baier, G., Ladeback, R., and Weigelt, G. 1985, *Astr. Ap.*, submitted.
Breysacher, J. 1981, *Astr. Ap. Suppl.*, **43**, 203.
Cassinelli, J. P., Mathis, J. S., and Savage, B. D. 1981, *Science*, **212**, 1497.
Cersosimo, T. C., and Loiseau, N. 1984, *Astr. Ap.*, **133**, 93.
Chu, Y. H. 1984, in *IAU Symposium 108, Structure and Evolution of the Magellanic Clouds*, ed. S. van den Bergh and K. S. de Boer (Dordrecht: Reidel), p. 259.
Chu, Y. H., Cassinelli, J. P., and Wolfire, M. G. 1984, *Ap. J.*, **283**, 560.
Conti, P. S., Leep, E. M., and Lorre, J. J. 1977, *Ap. J.*, **214**, 759.
Conti, P. S., Leep, E. M., and Perry, D. N. 1983, *Ap. J.*, **268**, 228.
de Boer, K. S., Koornneef, J., and Meade, M. R. 1981, in *The First Two Years of IUE* (NASA Conf. Publ., No. 2171), p. 771.
Ebbets, D. C., and Conti, P. S. 1982, *Ap. J.*, **263**, 108.
Feast, M. W., Thackeray, A. D., and Wesselink, A. J. 1960, *M.N.R.A.S.*, **121**, 337.
Feitzinger, J., and Isserstedt, J. 1983, *Astr. Ap. Suppl.*, **51**, 505.
Feitzinger, J. V., Schlosser, W., Schmidt-Kaler, Th., and Winkler, C. 1980, *Astr. Ap.*, **84**, 50.
Fitzpatrick, E. L., and Savage, B. D. 1984, *Ap. J.*, **279**, 578.
Freedman, W. 1984, Ph.D. thesis, University of Toronto.
Goss, W. M., and Radhakrishnan, V. 1969, *Ap. Letters*, **4**, 199.
Huchra, J. P., Geller, M. J., Gallagher, J., Hunter, D., Hartmann, L., Fabbiano, G., and Aaronson, M. 1983, *Ap. J.*, **274**, 125.
Inagaki, S., and Lynden-Bell, D. 1983, *M.N.R.A.S.*, **204**, 913.
Innes, R. T. A. 1927, *Southern Double Star Catalogue* (Johannesburg: Union Obs.).
King, I. R. 1962, *A.J.*, **67**, 471.
Koornneef, J., and Mathis, J. S. 1981, *Ap. J.*, **245**, 49.
Ledoux, P., Noels, A., and Boury, A. 1982, *Astr. Ap.*, **108**, 49.
Lequeux, J., Mancherat-Joubert, M., Deharving, J. M., and Kunth, D. 1981, *Astr. Ap.*, **103**, 305.
Massey, P., and Conti, P. S. 1983, *Ap. J.*, **273**, 576.
Meaburn, J., Hebden, J. C., Morgan, B. L., and Vine, H. 1982, *M.N.R.A.S.*, **200**, 1P.
Melnick, J. 1982, in *IAU Symposium 99, Wolf-Rayet Stars: Observations, Physics, Evolution*, ed. C. H. W. de Loore and A. J. Willis (Dordrecht: Reidel), p. 545.
———. 1983, *ESO Messenger*, No. 32, 11.
Mendoza, E. E. 1970, *Bol. Obs. Tonantzintla y Tacubaya*, **5**, 269.
Mihalas, D., and Binney, J. 1981, *Galactic Astronomy, Structure and Kinematics* (San Francisco: Freeman), p. 317.
Mills, B. Y., Turtle, A. J., and Watkinson, A. 1978, *M.N.R.A.S.*, **185**, 263.
Moffat, A. F. J. 1969, *Astr. Ap.*, **3**, 455.
———. 1983*a*, *Astr. Ap.*, **124**, 273.
———. 1983*b*, in *Proc. on Workshop Wolf-Rayet Stars: Progenitors of Supernovae?*, ed. M. C. Lortet and A. Pitault (Paris: Obs. de Meudon), p. V3.
———. 1985, in preparation.
Moffat, A. F. J., and Niemela, V. S. 1984, *Ap. J.*, **284**, 631.
Moffat, A. F. J., Niemela, V. S., Philips, M. M., Seggewiss, W., and Chu, Y. H. 1985, in preparation.
Moffat, A. F. J., and Seggewiss, W. 1983, *Astr. Ap.*, **125**, 83.
Moffat, A. F. J., and Shara, M. M. 1985, in preparation.
Peimbert, M., and Torres-Peimbert, S. 1974, *Ap. J.*, **193**, 327.
———. 1976, *Ap. J.*, **203**, 581.
Peterson, C. J., and King, I. R. 1975, *A.J.*, **80**, 427.
Phillips, M. M. 1982, *M.N.R.A.S.*, **198**, 1053.
Rosa, M. 1983, *Highlights Astr.*, **6**, 625.
Savage, B. D., Fitzpatrick, E. L., Cassinelli, J. P., and Ebbets, D. C. 1983, *Ap. J.*, **273**, 597.
Schommer, R. A., Olszewski, E. W., and Aaronson, M. 1984, *Ap. J. (Letters)*, **285**, L53.
Schweizer, F. 1979, *Ap. J.*, **233**, 23.
Sher, D. 1965, *M.N.R.A.S.*, **129**, 237.
Smith, L. J., and Willis, A. J. 1983, *Astr. Ap. Suppl.*, **54**, 229.
Spitzer, L., Jr. 1975, in *IAU Symposium 69, Dynamics of Stellar Systems*, ed. A. Hayli (Dordrecht: Reidel), p. 3.
van den Bergh, S., and Hagen, G. L. 1968, *A.J.*, **73**, 569.
van den Bos, W. H. 1928, *Bull. Astr. Inst. Netherlands*, **4**, 261.
Walborn, N. R. 1973, *Ap. J.*, **182**, L21.
———. 1984, in *IAU Symposium 108, Structure and Evolution of the Magellanic Clouds*, ed. S. van den Bergh and K. S. de Boer (Dordrecht: Reidel), p. 243.
———. 1985, private communication.
Walker, A. R., and O'Donoghue, D. E. 1984, preprint.
Weigelt, G. 1981, *Proc. ESO Conf., Scientific Importance of High Angular Resolution at Infrared and Optical Wavelengths*, ed. M. H. Ulrich and K. Kjar (Garching: ESO), p. 95.
Worley, C. E. 1984, *Ap. J. (Letters)*, **278**, L109.
Wray, J. D., and Corso, G. J. 1972, *Ap. J.*, **172**, 577.

A. F. J. MOFFAT: Département de physique, Université de Montréal, C. P. 6128, Succ. A, Montréal, PQ H3C 3J7, Canada

W. SEGGEWISS: Observatorium Hoher List der Universitäts-Sternwarte Bonn, 5568 Daun, F. R. Germany

M. M. SHARA: Space Telescope Science Institute, Homewood Campus, Baltimore, MD 21218

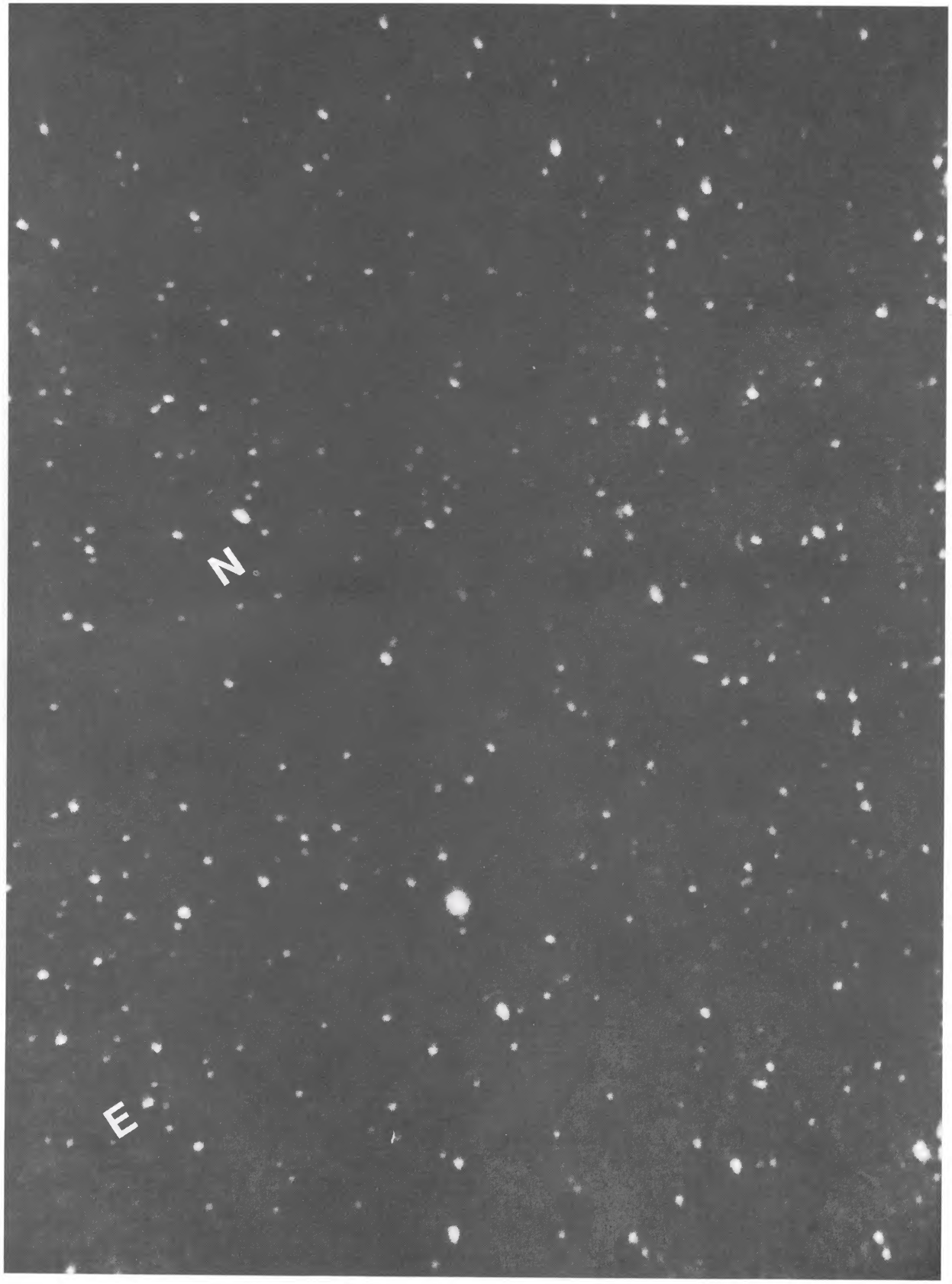

FIG. 1.—The field of view, approximately $15^\circ \times 18^\circ$, subtended by the SEC Vidicon camera utilizing a 105 mm *f*/0.7 lens during the Airborne Expedition. The video frame shown was recorded during the period of maximum brightness exhibited by β Cam, which appears at left center.

WDOWIAK AND CLIFTON (*see* page 171)